Ground heat exchanger thermal imbalance prevention; feasibility, development, and implementation

Connor Mitchell Dacquay

2022

Graduate School of International Resource Sciences, Akita University

Abstract

This research presents the outcomes from two main objectives with the first being the creation of a novel design of integrating electrochromic glass window controls with a GSHP system for long-term optimization and sustainability. For the first objective, a building energy model was developed and simulated with the solar heat gain coefficients of 0.41, 0.25, 0.15, and 0.09 to model electrochromic glass windows. The energy model outputs were used for ground heat exchanger model simulations which analyzed 20-year temperature trends and system efficiencies. The results showed that the integrated GSHP system with electrochromic windows was feasible and a conceptual control sequence and design was developed. The annual cooling demand decreased by 32% between the clear glass and fully tinted state. It was recommended to increase the ground heat exchanger capacity to 200 boreholes at 45.7 m in 2040 to prevent overheating from projected climate change. The average system coefficient of performance was 7.6 for the fully tinted window state. The integrated GSHP system reduced CO_2 emissions by 30% and the 30-year NPV was US$142,273.65 (-26%) cheaper compared to a conventional boiler and chiller system.

The second objective comprised of the development of a novel software and hardware package that dynamically predicts future ground heat exchanger temperatures to avoid thermal imbalance and future ground source heat pump system failure. An energy meter was installed on the ground heat exchanger of an office building and a software was created on a remote server that collected the measured data. The future ground temperature was dynamically calculated, and the prototype was integrated with the building automation system to prevent future ground source heat pump system failure. The results showed that the building was cooling dominate and if the current mechanical system operation continued, the system would become inefficient in 16 years from high inlet temperatures to the heat pumps. A control sequence was developed for mitigating ground heat exchanger failure on the studied building. It was

also determined by adjusting the set-point temperature of the make-up air unit from 12.8°C to 4.8°C, the amount of heating performed by the ground source heat pump system would increase from 81,122 kWh to 120,453 kWh which maintained the calculated 20-year ground heat exchanger temperature below 32°C. The prototype developed in this paper is critical for maintaining an efficient ground source heat pump system and adequate ground heat exchanger temperatures. The outcome of the second objective provides the solution of ensuring a successful adoption of sustainable green technology on a large scale and eliminates ground source heat pump system failure due to thermal imbalance.

Acknowledgments

I'd like to thank the love of my life Jessika Dowhanik and all my friends and family for supporting me throughout the journey of accomplishing my doctorate. I'd also like to thank Hikari Fujii, Shigemi Naganawa, Tsuyoshi Adachi, Hartmut Holländer, and Ed Lohrenz for acting as exceptional mentors throughout this process. I have learnt a remarkable amount from you all and for that, I am extremely grateful.

Table of Contents

List of Tables

List of Figures

Chapter 1 – Introduction

1.1 Overview

Fossil fuel combustion is driving climate change and has warmed Earth's global average temperature by 1.1°C since pre-industrial times (United Nations, 2019). Ground source heat pump (GSHP) systems have emerged as the most efficient way to heat and cool a building electrically due to its high energy saving potential (Sarbu & Sebarchievici, 2014). The most common GSHP systems work by leveraging the constant ground temperature and circulating heat exchange fluid through pipes buried in the ground. The pipes buried in the ground are commonly termed ground heat exchangers (GHX) which are connected to heat pumps located in a building. Proper design methodology for GSHP systems is relatively new, tedious, and time-consuming which leads to systems often failing because shortcuts are taken during the design process. In an effort to analyze how GSHP systems work, many researchers have modelled the performance of GHX's based on static load sets but few have focused on modelling the future performance based on monitored energy flow into and out of a GHX (Koohi-Fayegh & Rosen, 2015, 2021; Yang, Liang, Shi, & Chen, 2014).

A common problem with GSHP systems is the thermal imbalance between the amount of heat rejected to the ground versus the amount of heat extracted in the cooling and heating operations, respectively. Thermal imbalances in GSHP systems lead to the deterioration of mechanical system performance due to high heat pump inlet temperatures in a cooling dominate building or low heat pump inlet temperatures in a heating dominate building (You, Wu, Shi, Wang, & Li, 2016). Many researchers have analyzed the reduction in system efficiency based on thermal imbalances (Dai et al., 2015; J. Hwang, Song, & Lee, 2020; Qian & Wang, 2014; Shang, Dong, & Li, 2014; You, Wang, Wu, Shi, & Li, 2015), but none have dynamically calculated the future thermal imbalance based on real time energy loads.

Monitoring the live energy exchange to and from the GHX can notify building operators when a GSHP system has a thermal imbalance (Montagud, Corberán, Montero, & Urchueguía, 2011). Utilizing instrumentation such as energy meters on a GHX can mitigate system efficiency decline by notifying building operators of ground temperature drift.

1.2 Ground-source heat pump systems

Ground source heat pumps (GSHP) use electricity and the process of refrigeration to heat and cool buildings while utilizing a ground heat exchanger (GHX). GSHP's have been installed increasingly at a growth rate of 3.7% annually from 2015 to 2020 in the U.S. (Lund & Boyd, 2020). In recent years, several studies on cost and energy reduction were published for hybrid GSHP (HGSHP) compared to traditional GSHP systems (Alaica & Dworkin, 2017; Beckers, Aguirre, & Tester, 2018; Wang, Cui, Zhang, Zhou, & Li, 2017; Zhou et al., 2020) however, none of the studies focused on dynamically controlling building space heating and cooling loads to optimize the GSHP performance. GSHP systems act as a battery with a rechargeable source of energy based on the energy extraction and injection from the GHX. Utilizing technologies such as electrochromic (EC) glass to indirectly recharge the GHX for optimization is a novel concept and critical for sustainable future designs.

1.3 Objectives

The first objective of this thesis was to evaluate the mitigation of long-term thermal imbalance and optimizing the performance of a GSHP system by integrating EC window glazing controls. Additionally, the change in building energy demand based on the variable solar heat gain coefficient (SHGC) of the EC windows, impact of climate change, hourly system efficiencies, annual CO_2 emission reductions

and lifetime operating cost savings are also investigated. The outcome of this first objective will result in a follow up study involving the creation of a dynamic monitoring system that can integrate into the building automation system to control discretionary heating and cooling loads such as EC windows.

The second objective of this thesis was to create a GSHP energy meter integrated with a cloud-based analysis tool that monitors heat exchange fluid temperatures to and from a GHX, monitors flow rates through the GHX, calculates the net energy in and out of the GHX, predicts the future performance of the GHX based on the measured energy flow to/from the GHX on a commercial building, diagnoses the possibility of future system failure based on current operation, and integrates with the local building automation system. As the world transitions to heat pump technology amid a climate change crisis, GSHP systems have been adopted as the front runner and policy makers have introduced incentive programs to accelerate the adoption (Cuomo, 2021). Due to a lack in design knowledge in the GSHP industry, it is common for systems to fail due to temperature drift over time. As more GSHP systems are adopted, the prototype developed in this paper is critical for maintaining an efficient system and adequate ground loop temperatures. If monitoring systems are not introduced and GSHP systems fail on a grand scale, policy makers/governments will become uninterested in the technology. The second objective provides the solution of ensuring the successful adoption of GSHP technology on a large scale and eliminates GSHP system failure due to thermal imbalance.

The first objective determines the feasibility of controlling the long-term thermal balance of a GHX and acts as a proof of concept for developing a system that can provide the control. The second objective covers the creation and implementation of the system that provides the control for the long-term thermal balance of a GHX.

Chapter 2 – Literature Review

2.1 Climate change

In the United States (U.S.), commercial building energy usage accounts for 12% of all energy consumption (U.S. Energy Information Administration, 2019). 39% of the energy source in commercial buildings is currently supplied by fossil fuels. Out of the total commercial building energy usage, 25% of the energy consumption is space heating and 9.4% is space cooling (U.S. Energy Information Administration, 2012). The rise of fossil fuel emissions throughout the 19th and early 20th century has caused rising concerns regarding climate change.

The United Nations Framework Convention on Climate Change (UNFCCC) has predicted catastrophic outcomes if the global average temperature rises 2 °C above pre-industrial levels, as outlined in the 2015 Paris Agreement (United Nations, 2019). The global average temperature rise is directly caused by greenhouse gas emissions. Today, the world is 1.1 °C warmer than in pre-industrial times. Rising sea levels, retreating ice caps, and dying coral are the most visible impacts of a warming planet (United Nations, 2019). To reduce carbon emissions and therefore climate change, the electrification and decrease in energy usage of commercial buildings is critical.

2.2 Hybrid ground source heat pump systems

EC glass or smart glass is a technology that applies a low voltage of electricity that darkens a glass coating as lithium ions and electrons transfer from one EC layer to another which adjusts the solar heat gain coefficient (SHGC). EC glass has been adopted as a building construction technology that can be applied instead of conventional windows and has been projected to save 10^{15} J in the year 2030 compared to a low emittance window if it reaches 40% market penetration level in the U.S. commercial

building sector (Lee, Yazdanian, & Selkowitz, 2004). Serveral studies showed that EC windows in commercial buildings can manipulate space conditioning loads and generate energy savings (DeForest et al., 2015; Fernandes, Lee, & Ward, 2013; Javad & Navid, 2019; Oh, Tae, & Hwang, 2018; Tavares, Bernardo, Gaspar, & Martins, 2016). Yet, none of the papers used EC windows to manipulate space conditioning loads to manipulate building energy loads to prevent long-term thermal imbalance of a GSHP. One study looked at the sizing of a cooling tower for a hybrid ground source heat pump (HGSHP) system for an office building and the affect of changing the SHGC of the window glazing by using validated numerical modelling but failed to analyze the long-term sustainability and optimization (Sagia, Rakopoulos, & Kakaras, 2012). HGSHP systems are often thought of as GSHP systems with either a supplementary heating or cooling device strictly used to reduce capital cost and mitigating long-term temperature imbalance of the subsurface to ensure high efficiencies. This concept of balancing heating and cooling loads for a sustainable and high performing GSHP system can be extended to other supplementary technologies such as solar water heaters, snow melt systems, ice storage systems and fluid coolers. However, a device such as EC window glazing which is not a supplementary heating or cooling device has not been considered for a HGSHP system. The key question remains if EC window glazing can be used to optimize the performance of a GSHP system by manipulating building space heating and cooling loads and if a GHX monitoring system can diagnose the possibility of future system failure and integrates with the local building automation system to prevent long term GHX thermal imbalance.

2.3 Energy meters

Energy meters are comprised of a flow meter and two temperature sensors on the inlet and outlet of the GHX (Meyerson, 1967). Numerous researchers have collected and studied the real time energy loads

from an energy meter on a GSHP system, (Y. Hwang et al., 2009; Li, Nagano, Lai, Shibata, & Fujii, 2013; Luo et al., 2015; Michopoulos, Zachariadis, & Kyriakis, 2013; Safa, Fung, & Kumar, 2015; Yan et al., 2016), but none have dynamically calculated the future system GHX temperatures based on real time energy loads. Recently, researchers have focused on artificial intelligence (AI) for optimizing geothermal systems (Zhao et al., 2020). Khosravi and Syri (2020) used AI to optimize the efficiency of a hybrid geothermal power plant system but did not focus on geothermal heat pump applications. Although there has been research based on the data collected from monitoring GSHP systems, in practice, energy meters installed on GHX's are uncommon. If a GSHP system is installed with an energy meter, the data is often neglected and unused.

Stephen Hamstra (2019) introduced the concept of using an energy meter for dynamic GSHP efficiency optimization but did not focus on calculating future temperature trends to avoid system failure. The ability to identify future thermal imbalance of a GSHP system from an off-site server eliminates human error in data collection and allows for an automated alert system to prevent foreseeable temperature drift. The key question remains whether it is possible to dynamically calculate long-term GHX temperatures on a remote server based on measured energy data to prevent system failure. This study is the first to develop a software and hardware package that dynamically calculates future GHX temperatures to avoid thermal imbalance and future system failure.

Chapter 3 – Feasibility of thermal load control from electrochromic windows for ground heat exchanger thermal imbalance prevention

3.1 Methodology

EC glass or smart glass is a technology used as commercial building windows that can manipulate space heating and cooling energy loads. To optimize a GSHP system, the balance between building space heating and cooling loads is needed. In this study, we integrated the EC windows and GSHP system by developing four building energy models with the solar heat gain coefficients of 0.41, 0.25, 0.15, and 0.09 to model the EC glass windows. Additionally, four weather files were used to create the energy load sets: the typical meteorological year weather file, projected 2050 weather for RCP 2.6, RCP 4.5, and RCP 8.5 climate change scenarios. The building energy model outputs were used for GHX model simulations which analyzed 20-year temperature trends and system efficiencies.

3.1.1 Numerical simulation method

This study was based on an office building located in Perham, Minnesota, US (Fig. 1). The 4-storey office building had an expected gross floor area of 7154 m^2 after the addition was complete and exterior window to wall ratio of 28.8% and was equipped with a GSHP system and vertical GHX. The original vertical GHX was built in 1998 and consisted of 160 U-tubes spaced at 2.4 and 3.1 m with 2 U-tubes in series (Fig. 2). Since then, 20 U-tubes have failed therefore, the GHX consists of 140 working U-tube boreholes. The U-tubes had a 21.6 mm inner diameter (ø) composed of standard dimension ratio (SDR) of 11 high-density polyethylene (HDPE) pipe. 10 U-tubes were connected to supply and return runouts that were 51.0 mm ø SDR 13.5 HDPE pipe which were connected to a main manifold that was 119.5

mm ø SDR 13.5 HDPE pipe. There were supply and return runouts that connect the main manifold to the studied office building.

Trane Trace 700^{TM} building energy modelling software (Trane, 2019) was used to determine the hourly space heating and cooling block loads in kW based on the proposed building design. Next, a simulation was run with alternatives where the solar heat gain coefficient of the buildings windows was changed to 0.41, 0.25, 0.15, and 0.09 to analyze the impact on space heating and cooling loads. The impact from projected climate change was then analyzed by using the Model for Interdisciplinary Research on Climate (MIROC5) global atmospheric general circulation model (GCM) for the climate change representative concentration pathways (RCP) 2.6, RCP 4.5, and RCP 8.5 (Figure 3). RCP 2.6 required that CO_2 emissions start declining by 2020 and are eliminated by 2100 which creates the radiative forcing level of 3.1 W/m^2 by 2050 and decreases to 2.6 w/m^2 by 2100. RCP 4.5 was a stabilization scenario in which total radiative forcing is stabilized shortly after 2100 to 4.5 W/m^2. RCP 8.5 was characterized by increasing greenhouse gas emissions over time, with a rising radiative forcing of 8.5 W/m^2 by 2100. To down-scale the monthly MIROC5 data to hourly data for the year 2050, a morphing method was applied to the typical meteorological year (TMY) file from the Fergus Falls municipal airport weather station (Wan, Li, Pan, & Lam, 2012). To scale the wet-bulb temperature based on the dry-bulb temperature and relative humidity (RH), the empirical equation developed by Stull (2011) was used. The energy load sets were then created using the future climate data and changing the SHGC of the building windows to 0.41, 0.25, 0.15, and 0.09.

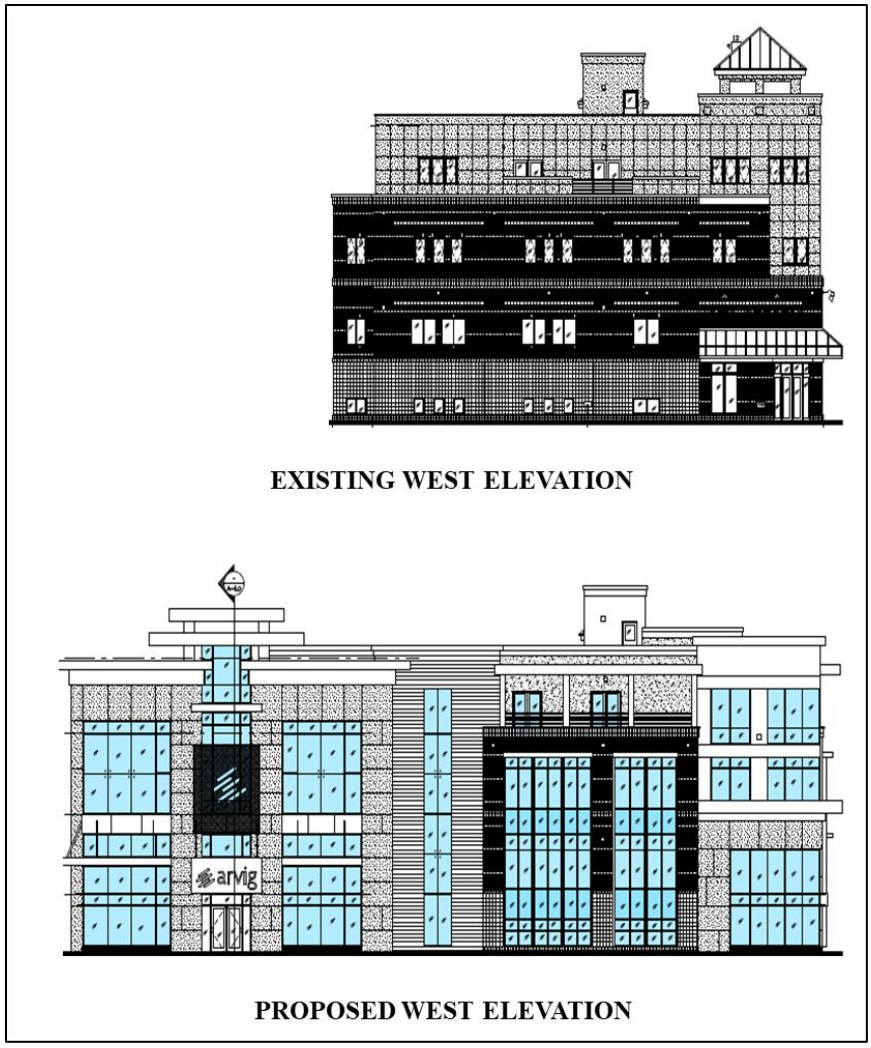

Figure 1: Proposed and existing West elevation of studied building.

Ground Loop Design™ (Gaia Geothermal, 2020) software was used to determine the hourly and 20-year projected GHX performance based on the various energy load sets. The maximum entering water temperature (EWT) to the heat pumps were analyzed to determine the 20-year sustainability of the GSHP system based on the existing GHX size. Additionally, the hourly EWT was analyzed for the energy load sets with SHGC of 0.41 and 0.09 to determine a preliminary control sequence for the integrated GSHP system with EC windows. The energy load sets with the future climate data and variable

window SHGC were used to analyze the max 20-year EWT and the projected year the GHX overheated (T_{OH}). The additional size of GHX needed to maintain sustainable operation through 2050 was then determined. The hourly coefficient of performance (COP) was calculated for the energy loads sets with the SHGC of 0.41 and 0.09 to analyze the change in efficiency for heating, cooling, and simultaneous loads, based on the variable solar heat gains. To calculate the hourly COP's, the Carnot equations were used (Callendar, 1911):

$$COP = \frac{Q_H}{W_{in}} \quad (1)$$

where COP is the coefficient of performance, Q_H is the desired output in kW and W_{in} is the work required in kW. Projected energy savings were then determined by comparing the GSHP system with integrated EC windows versus a conventional chiller and natural gas boiler system with standard building code windows using a U-value of 0.28 and SHGC of 0.41 (Energy Star, 2020). The projected cost savings were determined using standard commercial natural gas rates 12.5 ¢/m^3 (Perham Natural Gas, 2020) and electricity rates of 7.12 ¢/kWh for June to September and 7.47¢/kWh during October to May (OTPCO, 2020b). The CO_2 emissions were calculated by using standard natural gas emissions (United States Environmental Protection Agency, 2017) and an electricity emissions intensity of 0.77 kg/kWh (OTPCO, 2020a). Lastly, the net present value (NPV) for the operating lifetime of the GSHP system integrated with EC windows was calculated by solving for the present worth based on the equal operating cost payments made at the end of every interest period for the lifetime of the system and considering the effects of inflation:

$$P = \frac{C}{1+g}\frac{(1+r)^n-1}{r(1+r)^n} \quad (2)$$

where C is the annual energy cost savings in the first year in US$, n is the project lifetime in years, r is the real interest rate, g is the average inflation rate in the US from 2000-2019 taken as 2.18% (US

Inflation Calculator, 2020). The Fisher Equation was used to calculate the real interest rate based on the nominal interest and inflation rate from the following:

$$r = \frac{1+i}{1+g} - 1 \quad (3)$$

where i is the average interest rate in the US from 2000-2019 taken as 2.24% (FRED, 2020).

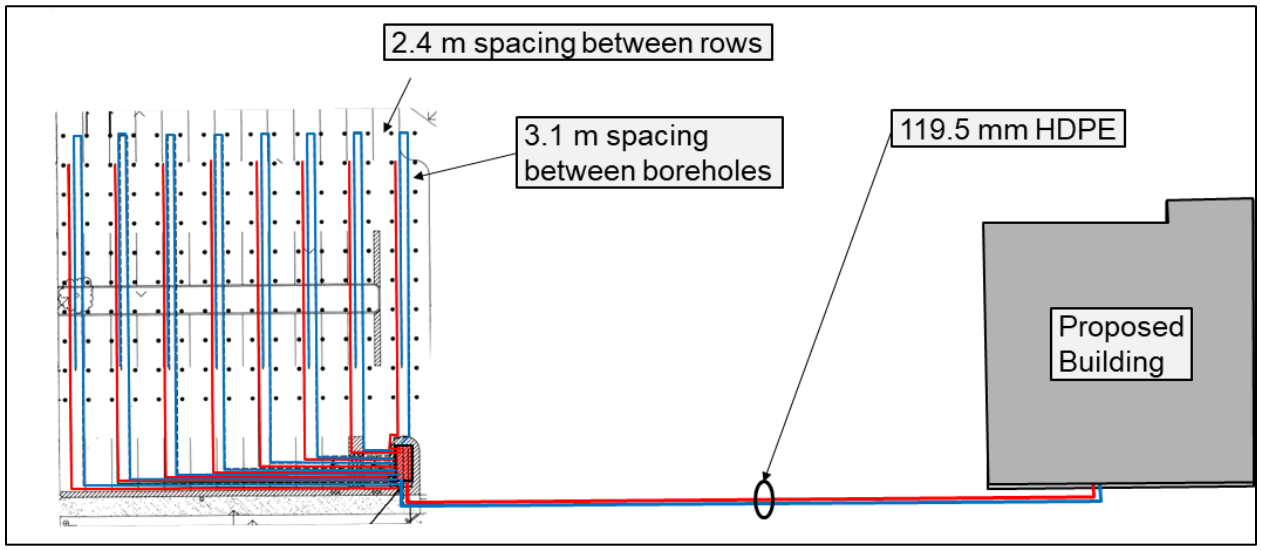

Figure 2: Schematic of existing ground heat exchanger.

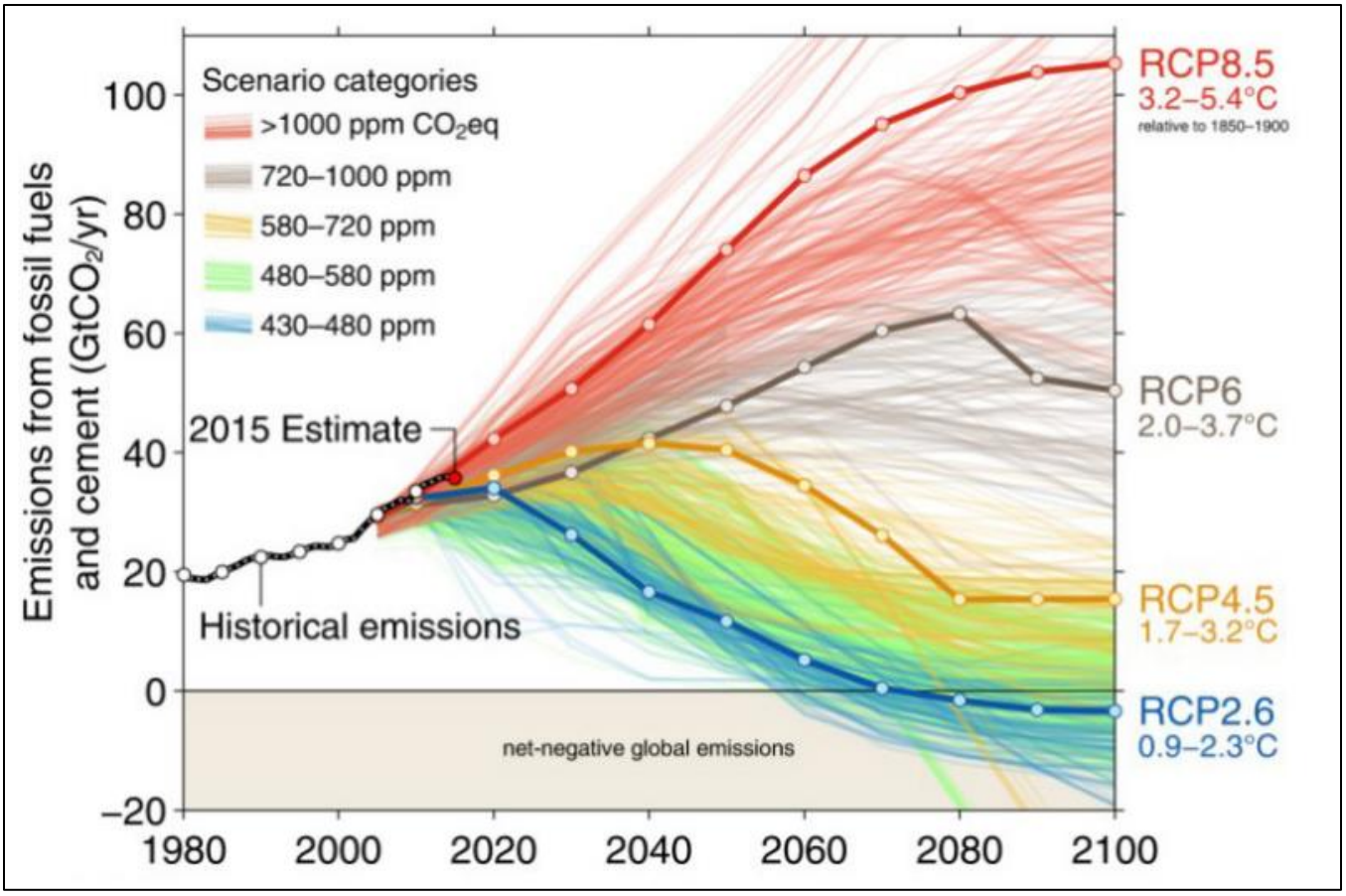

Figure 3: Carbon dioxide emission pathways until 2100 (Craik, 2017).

3.1.2 Model assumptions

In this study, it was assumed that the natural gas boiler efficiency was 90% and centrifugal chiller EER was 20 (ASHRAE, 2016) for the calculation of the conventional systems operating costs. It was also assumed that the operating life of a GSHP was 20 years (U.S. Department of Energy, 2011). An isotropic subsurface condition and constant thermal properties of 2.08 W/m/K for thermal conductivity and 0.093 m^2/day for thermal diffusivity with a constant ground temperature of 8.9°C were assumed based on a site-specific thermal response test. Line source theory was used for the GHX calculations which assumes purely conductive heat transfer (Eskilson, 1987). The temperature of the borehole was calculated by using:

$$T_b(t) = T_{om} - \frac{q}{(2\pi\lambda)g(t/t_s, r_b/H)} \text{ where } t_s = \frac{H^2}{9a} \quad (4)$$

where T_{om} is the effective undisturbed ground temperature in K, q is the average heat extraction rate over the borehole in W/m, λ is the thermal conductivity in W/m/K, t is time in days, t_s is steady-state extraction time in days, r_b is the borehole radius in m, a is the thermal diffusivity in m^2/day and H is the borehole length over which heat extraction takes place in m. It was also assumed that the projected change in annual mean surface air temperature by 2050 was 1.5°C and 2.3°C for RCP 2.6 and RCP 8.5 respectively (Bush and Lemmen, 2019) for Perham, MN. For calculating the lighting energy savings from the EC windows, an average energy consumption reduction of 55% was assumed based on the study conducted by Fernandes et al. (2013). It was assumed that the heat pump EWT is unacceptable when greater than 35°C and less than 2°C due to poor performance and equipment limitations (Kavanaugh & Rafferty, 2014). This assumption governed the year at which the GSHP system overheated and ultimately failed (T_{OH}). It was assumed that the flow type within the U-tubes was transitional flow based on calculated Reynolds numbers. The flow rate was also assumed as 3.2 L/hr/kW based on standard design (Kavanaugh & Rafferty, 2014). The assumed indoor design conditions were 23.3°C for cooling and 21.7°C for heating based on the ASHRAE-55 standard (ASHRAE, 2017). The assumed ventilation rates for the various room types in the energy model were based on the ASHRAE-62.1 standard (ASHRAE, 2016). For calculating the NPV, it was assumed that the product life of EC windows is 30 years (SageGlass, 2020b).

3.1.3 Parametrization

For the building energy model, window glass properties were used from standard values from SageGlass with a U-factor of 1.6 W/m^2·K. The various tint levels were classified as clear glass for a SHGC of

0.41, semi-clear for a SHGC of 0.25, semi-tinted for a SHGC of 0.15 and fully tinted for a SHGC of 0.09 (SageGlass, 2020c). The building envelope insulation was based on the Tables 5.5-1 to 5.5-7 in ASHRAE 90.1 (2016) for climate zone 6a and Table 1 shows the corresponding room type and internal load information for the energy model. The data room equipment energy was consumed 100% of the time but all other room type occupancy, lighting, and equipment hourly schedules were based on information gathered from the office building staff. The hourly schedules were based on operating times between 7 am to 6 pm during weekdays, 7 am to 4 pm on Saturdays and closed on Sundays.

Table 1: Room type with occupancy, lighting, and equipment internal load density information.

Room type	Internal Load Density		
	Occupancy	Lighting (W/m^2)	Equipment
Café	1 m^2/person	8.6	0 W/m^2
6-Person Conference Room	6 people	8.6	2.7 W/m^2
10-Person Conference Room	10 people	8.6	2.7 W/m^2
18-Person Conference Room	18 people	8.6	2.7 W/m^2
Corridor/Vestibule	0 people	8.6	0 W/m^2
Data Room	0 people	8.6	1.8 kW
Gym	1.9 m^2/person	8.6	5.4 W/m^2
General Office Space	18.6 m^2/person	8.6	125 W/workstation
Kitchen	18.6 m^2/person	8.6	16.1 W/m^2
Laboratory	3.1 m^2/person	8.6	5.4 W/m^2
Lecture Hall	169 people	8.6	0 W/m^2
Mechanical Room	0 people	8.6	10.7 W/m^2
Storage	0 people	5.4	0 W/m^2
Toilets	0 people	8.6	1 W/m^2

For the GHX model, the heat exchange fluid was taken as 20% propylene glycol and water blend whereas the other main parameters used can be seen in Table 2. These values were based on the as-built specifications.

Table 2: GHX design parameters used in Ground Loop Design™.

Parameter	Value
Borehole number	140
Vertical borehole separation	2.4 m
Horizontal borehole separation	3.1 m
Borehole diameter	102 mm
Borehole depth	45.7 m
Borehole thermal resistance	0.24 m·K/W
Radial pipe placement	Average
Design flow rate	3.2 l/hr/kW
Flow type	Turbulent
Ground thermal conductivity	2.08 W/m/K
Ground thermal diffusivity	0.093 m^2/day
Grout thermal conductivity	0.726 W/m/K
Undisturbed ground temperature	8.9°C
Prediction time	20 years
Pipe type	SDR11
U-tube inside diameter	21.8 mm
U-tube outside diameter	26.7 mm

3.1.4 Model validation

The building analyzed in this study did not have current energy consumption data to calibrate the energy model since the anticipated addition had not been built. To validate the building energy model used in this study, a case study for a similar type office building in a similar climate was used. Trane Trace 700^{TM} building energy modelling software (Trane, 2019) was used to calibrate an energy model compared to the existing energy consumption of the building. The 1037 m^2 office building was located in Fergus Falls, Minnesota, US, which has a ASHRAE climate zone 6a, and the monthly energy consumption for electricity and natural gas can be seen in Table 3. The energy model was developed using hourly weather data for a typical meteorological year, mechanical and civil construction drawings, and design specifications. The modelled annual natural gas usage matched the measured usage within 0.7% whereas the modelled annual electricity usage matched the measured usage within 0.9%. The accuracy between the measured energy consumption and the simulated energy consumption validated the energy model used in this study.

Table 3: Comparison of measured and modelled energy consumption for office building in ASHRAE climate zone 6a.

Month	Measured Natural Gas Usage (m^3)	Modelled Natural Gas Usage (m^3)	Measured Electricity Usage (kWh)	Modelled Electricity Usage (kWh)
Jan	3,480	2,976	6,575	4,277
Feb	2,028	2,672	4,887	3,928
Mar	3,192	2,310	5,805	4,631
April	1,304	1,167	4,720	4,872
May	489	690	4,190	5,674
June	170	290	4,809	6,857
July	36	82	5,703	8,463
Aug	52	44	6,208	8,979

Sept	129	167	6,699	6,650
Oct	893	819	5,825	4,851
Nov	1,499	1,411	6,432	4,356
Dec	1,722	2,266	6,501	4,235
Total	14,993	14,895	68,354	67,773

3.2 Results and discussions

3.2.1 Impact of SHGC on energy loads

An analysis was performed on the variable SHGC on the EC windows to determine the change in space cooling and heating energy loads of the studied office building. The results showed that the annual cooling load decreased by 32% between the clear glass state (SHGC = 0.41) and the fully tinted state (SHGC = 0.09). Additionally, there was a correlation of 0.99 between the decrease in cooling load and the decrease in SHGC which can be seen in Fig. 4. This showed that the solar radiation penetrating through the windows into the building was blocked due to the lower SHGC which therefore contributed to less space cooling needed to create thermal comfort within the office.

Although the U-factor for the windows was kept constant for the various simulations, the impact of the variable SHGC was significant and showed consistent results with the study performed by Oh et al. (2018). The authors concluded that the cooling load reduced by 29% between the clear and EC colored state window for a high-rise residential building which verifies the results produced by the numerical model in this study. The heating load showed an opposite affect compared to the cooling load with an increase of 14% between the clear and fully tinted state. With the reduction of solar heat gains, an average of 81 kWh/day of commercially supplied energy was needed to supplement the office to achieve

thermal comfort. Since a GSHP system is dependent on the heat exchange surface area between the GHX and the surrounding soil, additional energy cannot be provided as easily compared to a conventional natural gas or electric system. The soil mass is a finite energy source and the balance between the energy extracted to and from the subsurface is critical for long-term high efficiency operation for a GSHP system.

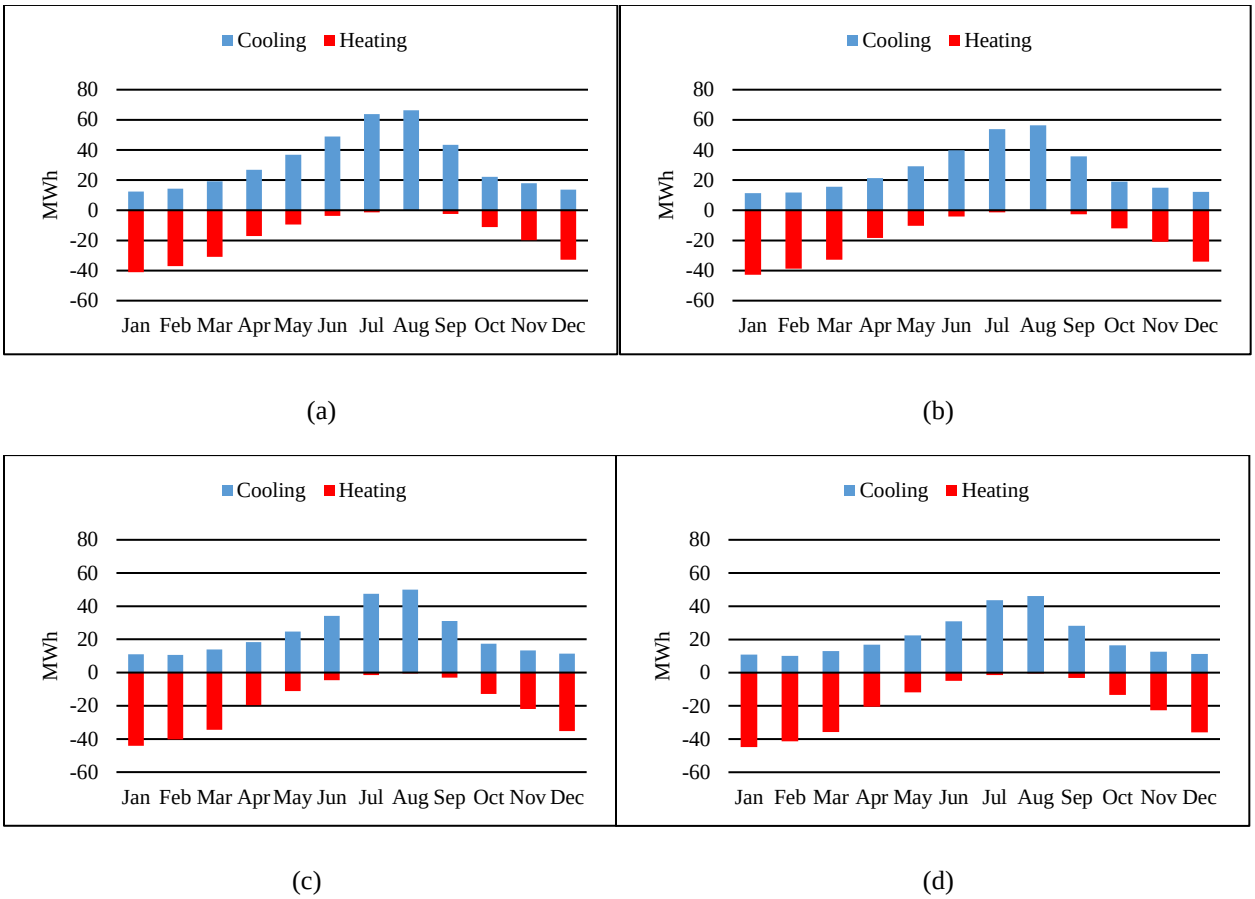

Figure 4: Monthly space heating and cooling energy demand in MWh for: (a) window SHGC of 0.41, (b) window SHGC of 0.25, (c) window SHGC of 0.15, and (d) window SHGC of 0.09.

3.2.2 Long-term GSHP system performance

To determine whether the existing 140 U-tube bore field could provide the space heating and cooling for the added floor area for the studied office building, a 20-year projection of heat pump EWT's was

analyzed based on the energy loads previously discussed. All scenarios began the simulation with the ground temperature based on the annual average ambient air temperature of 8.9°C. Fig. 5 shows that when the windows are in a clear state, the GSHP system will overheat by the 5th year of operation and throughout the 20-year operation, had a maximum EWT of 65.9 °C. The maximum acceptable EWT is shown by the red line plotted at 35°C. The overheating of the system was caused by the imbalance between heat injected to the GHX from space cooling in the building versus heat extracted for space heating. Similarly, when the SHGC is 0.25 and 0.15, the system will overheat by year 8 and 16, respectively. Throughout the 20-year operation life, the maximum EWT was 46.5°C for a SHGC of 0.25 and 36.6°C for a SHGC of 0.15. For the fully tinted state at SHGC of 0.09, the system gradually increases in temperature due to the imbalance between space cooling and heating but remained within acceptable range of heat pump operation with a maximum EWT of 31.5°C.

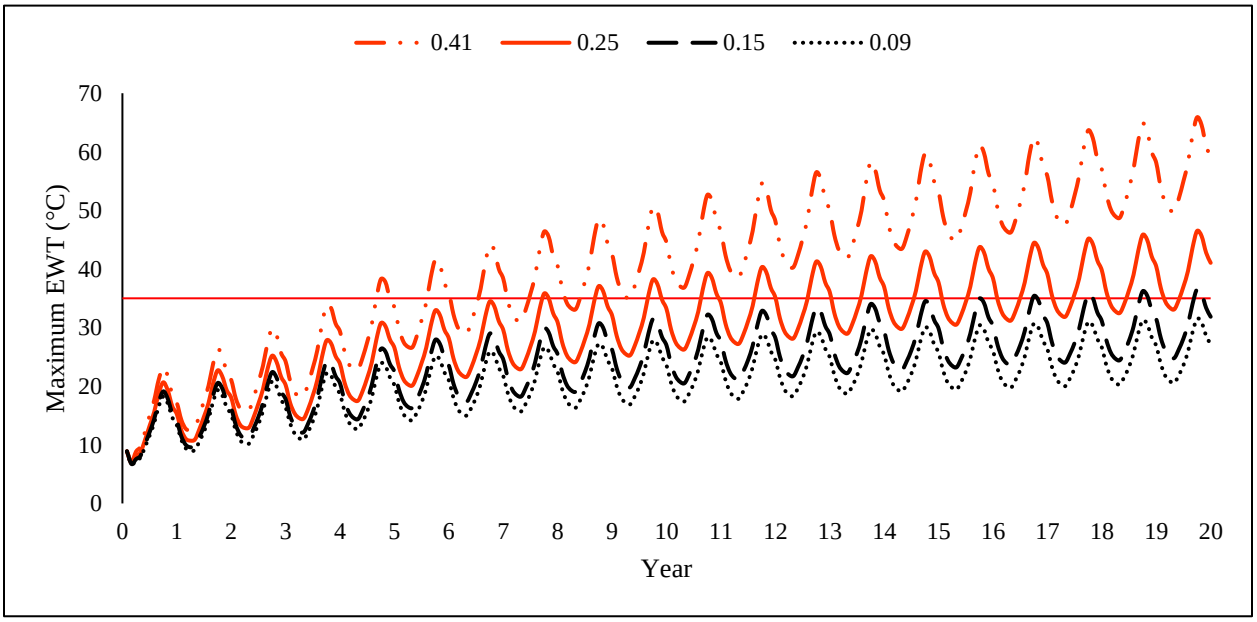

Figure 5: 20-year projection of the maximum EWT to the heat pumps for window SHGC of 0.41, 0.25, 0.15, and 0.09.

In all scenarios, the heat pump EWT increases annually regardless of the office building window SHGC. This is due to the consistent imbalance between annual heat rejected to the ground versus extracted. To eliminate the constant annual imbalance year after year, hourly controls of the window SHGC based on the heat pump EWT is necessary. Fig. 6 shows the hourly EWT's for the first year of operation for the fully tinted and clear window state. From the winter months of November to April, the average difference between the hourly EWT's is 1.7°C. Based on Fig. 4, the office building is heating dominant during the winter months. Since the 20-year temperature trend depicted an increasing EWT, the EC windows should be used in their full tint state throughout the winter months. This would decrease the amount of solar heat gain and increase the amount of heat extracted from the ground due to the additional heating needed to provide thermal comfort for the building occupants. This would reduce the increase in EWT over time and mitigate the thermal imbalance.

Throughout the summer months of May to September the EWT difference increases to 3.3°C. During the summer months the office building is heavily cooling dominant (Fig. 4) which means majority of the time the EC windows should be used in their full tint state to prevent the GHX from overheating. In the event of the energy extracted from the ground exceeds the amount of energy injected, the EC win-

dows should be switched to their clear state to increase the solar heat gains which would require additional cooling.

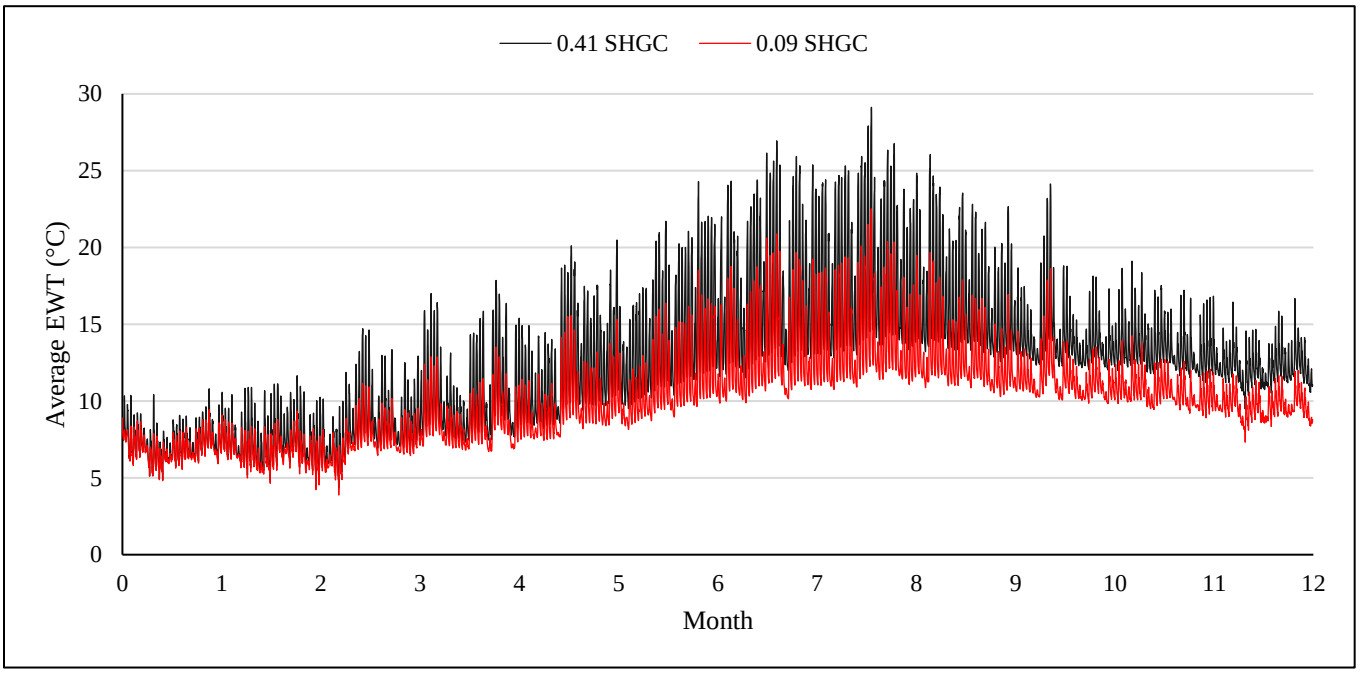

Figure 6: Hourly average EWT's to the heat pump for a 1-year operation with SHGC of 0.41 and 0.09.

Integrating EC glass controls to the GHX allows for the increase or decrease of solar heat gains into the building which can control the space heating and cooling demand. Two temperature sensors on the inlet and outlet of the GHX along with a flow meter can be installed to determine whether the ground temperature is decreasing or increasing outside of an allowable tolerance. This combination of sensors is defined as an energy meter because the energy extracted from the ground versus injected into the ground can be calculated (Meyerson, 1967). The energy meter can be connected to a remote server where long-term temperature trends can be collected and calculated (Fig. 6). Based on the temperature trends, the remote server can send signals to the client owned building automation system (BAS). The BAS can send signals to the EC controls via BACnet to either increase or decrease the tint of the EC windows.

The glass tint increments are defined by the four stages of SHGC: 0.41, 0.25, 0.15, and 0.09. A signal will be sent to the smart glass controls to decrease the glass tint by 1 increment when the temperature of the ground loop is less than the specified set point by 0.5°C. Conversely, a signal will be sent to increase the glass tint by 1 increment when the temperature of the ground loop is greater than the set point by 0.5°C. The minimum and maximum set points are defined as 2°C and 35°C, respectively (Kavanaugh & Rafferty, 2014). A 1°C difference from the set-points will signal the smart glass to either decrease or increase the tint by 2 increments and similarly for a 1.5°C difference until the maximum or minimum glass tint increment is reached. When the GHX temperature is within the pre-programmed set-points, the smart glass will be controlled by either façade or rooftop sky sensors for typical operation. The results discussed prove the feasibility of integrating EC controls with a GSHP system which will be implemented and covered in a follow up study.

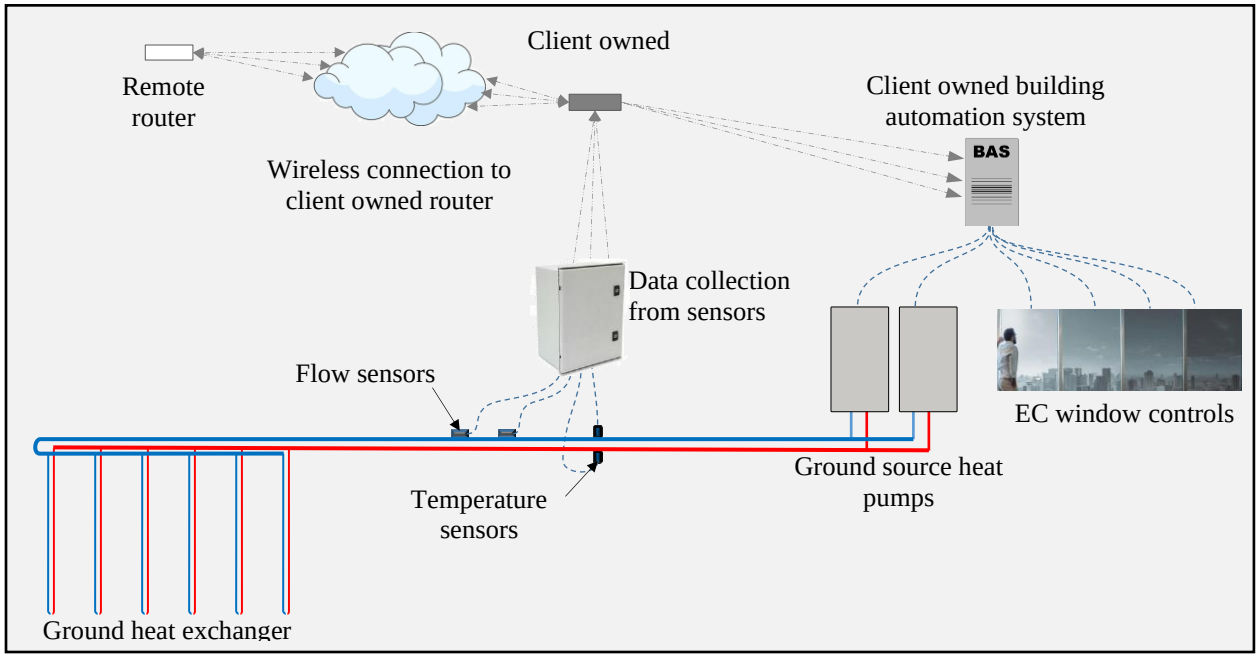

Figure 7: Conceptual design of integrated GSHP with EC window controls.

3.2.2.1.Impact of climate change

Although GSHP systems are typically designed for 20 years, the vertical GHX component is often used for 50 years; therefore, analyses based on different climate change scenarios was performed for the year 2050. Fig. 8 shows the hourly temperature difference of two climate change scenarios, RCP 2.6 and RCP 8.5 compared to the base climate data. The average change in ambient air temperature for the scenarios RCP 2.6, RCP 4.5, and RCP 8.5 were 0.3, 1.6 and 2.3°C, respectively. The change in ambient air temperature for RCP 2.6 was minimal whereas RCP 4.5 has an increase in temperature during winter months and decrease in temperature during summer months. RCP 8.5 has an increase in ambient air temperature throughout all seasons with the largest increase in the summer months.

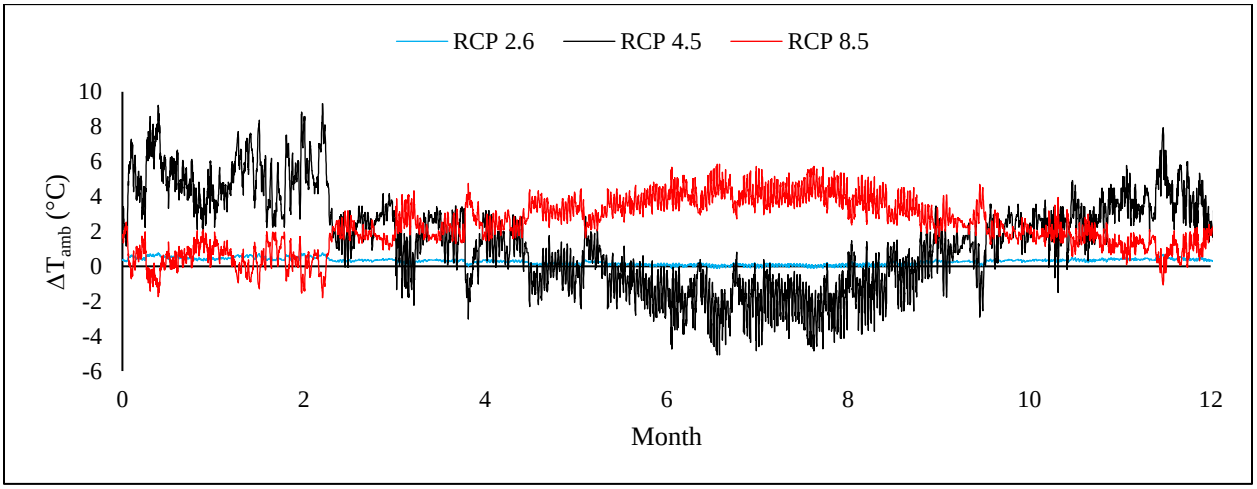

Figure 8: Hourly dry bulb temperature difference of climate change scenarios RCP 2.6, RCP 4.5 and RCP 8.5.

The change in projected temperature had an average space cooling demand increase for all tint levels of 9%, 6% and 24% for the climate change scenarios RCP 2.6, RCP 4.5, and RCP 8.5, respectively (Table 4). The space heating demand decreased an average of 1% for RCP 2.6, 22% for RCP 4.5, and 13% for RCP 8.5. These values are similar to a simulation performed in Harbin, China which is classified as

an ASHRAE 7 climate zone, where the projected heating load decreased 22.3% and cooling load increased 18.5% (Wan et al., 2012). This verifies the values produced in this study.

Although the solar radiation was not adjusted based on anticipated climate change, the change in space cooling demand was 2% and 6% between the clear window state and fully tinted state for RCP 2.6 and RCP 8.5, respectively. This indicates a negative relationship between solar radiation and change in space cooling demand. Since there was less solar radiation contributing to the space cooling when the windows were fully tinted, the space cooling demand is therefore more dependent on the change in outdoor air temperature which leads to the higher percentage change in cooling demand between the clear window state and fully tinted state.

The anticipated increase in ambient air temperature from climate change causes a greater imbalance between heating and cooling loads which causes the GHX to overheat faster than current weather conditions. After 20-years of operation the GHX is expected to have EWT of 91°C for RCP 8.5 and 73°C for RCP 2.6 and RCP 4.5 based on a SHGC of 0.41 (clear state). These EWT's are 25°C and 7°C higher than projections based on current weather conditions. For all climate change scenarios, the GHX T_{OH} was within 14 years for all window tint states. This shows a negative feedback loop between CO_2 emissions and GSHP operation which reinforces the importance of reducing CO_2 emissions to mitigate the impact from climate change.

Table 4: Percent change in cooling demand and heating demand, 20-year maximum EWT to the heat pumps and projected year to overhead for window SHGC of 0.41, 0.25, 0.15 and 0.09 based on climate change scenarios RCP 2.6, RCP 4.5, and RCP 8.5.

	RCP 2.6				RCP 4.5				RCP 8.5			
SHGC	0.41	0.25	0.15	0.09	0.41	0.25	0.15	0.09	0.41	0.25	0.15	0.09

% Change in Cooling	8	9	10	10	5	6	6	6	20	23	25	26
% Change in Heating	-0.6	-0.7	-1	-2	-21	-22	-23	-23	-11	-12	-13	-14
20-Year Max EWT (°C)	73	56	44	38	73	57	44	39	91	75	65	58
YOH (Yr)	4	6	9	14	4	6	9	13	3	4	5	6

The uncertainty of the future climate causes concerns for a GSHP system that has a limited and variable energy source, therefore it is recommended to increase GHX capacity to 200 boreholes at 45.7 m in 2040 when the life cycle of the heat pumps is complete. Although an assumption in this study was to neglect groundwater convective heat transfer which overestimates the recommendation, this ensures the max EWT to be below 35°C for a worst-case scenario of RCP 8.5 from 2040-2060. Lastly, the variability in weather data and energy loads shows the importance of integrating EC windows with the GSHP system to mitigate long-term temperature imbalance and increase operational flexibility within the system.

3.2.3 System efficiencies

The hourly COP's for heating, cooling and simultaneous demand were calculated based on the fully tinted and clear window state using current climate data (Table 5). The simultaneous COP was calculated by the total load divided by the greater of the heating or cooling power consumption.

Table 5: Hourly COP's for heating, cooling, and simultaneous demand for window SHGC of 0.41 and 0.09 using current climate data.

SHGC	0.41			0.09		
	Average	Max	Min	Average	Max	Min
Heating (COP)	5.3	33.4	1.1	6.4	33.9	1.3

Cooling (COP_C)	8.5	25.1	1.6	9.2	19.8	1.9
Simultaneous (COP)	7.5	27.2	2.0	7.3	23.4	2.1

The COP's for the fully tinted windows were 17% higher in heating, 8% higher in cooling, and 3% lower during simultaneous loads compared to the clear windows. This was attributed to the decline in power required from the heat pumps due to the reduction in cooling load because of the decrease in solar gains from the higher SHGC of the office building's windows. The reduction in cooling load created less heat rejection to the GHX which lowered the EWT's to the heat pump. The lower the EWT's, the less energy the heat pumps needed to run more efficiently to provide the adequate building side water temperatures.

The simultaneous COP was higher for the clear window state because during the spring and fall seasons, the additional solar heat gains create an energy balance with less heat pump energy being required. In the case of the tinted window state, the solar heat gains are reduced due to the lower SHGC, which required the heat pump to provide an additional heating load. The higher average heating and cooling COP for the tinted window state combined with the higher simultaneous COP for the clear window state shows the advantage of integrating EC glass controls with the GHX to provide the highest efficiency for the system throughout the year.

3.2.4 CO_2 emission and cost savings

The annual projected energy costs for space heating, space cooling, and lighting were calculated for the integrated GSHP system with EC windows and a conventional natural gas boiler and chiller system using ASHRAE standard efficiencies and the hourly COP's previously calculated based om the simulated hourly energy loads. The annual projected costs for the conventional and integrated GSHP system

are US$19,656 and US$14,647 respectively with the monthly energy consumption shown in Table 6. Additionally, the conventional system is projected to emit 218 tonnes of CO_2 eq. while the integrated GSHP system reduced the emissions by 30% to 154 tonnes of CO_2 eq.

Table 6: Projected monthly energy consumption for a conventional system versus the GSHP system with integrated EC windows.

	Conventional		GSHP
	kWh	m^3 NG	kWh
Jan	15,818	4,384	11,880
Feb	14,923	3,951	11,048
Mar	17,762	3,296	13,343
Apr	17,948	1,825	15,525
May	20,377	1,011	19,344
Jun	22,291	403	25,852
Jul	24,417	141	25,517
Aug	25,811	43	19,794
Sep	20,780	266	17,702
Oct	17,874	1,182	14,262
Nov	16,612	2,131	13,412
Dec	15,835	3,502	12,542
Total	230,448	22,135	200,221

The energy cost savings are relatively low due to the current cost of natural gas. As natural gas prices increase or carbon taxes are implemented, the cost savings of electrifying the office building will increase proportionally. The additional benefit to electrifying the building is the elimination of on-site

CO_2 emissions and the continuing decrease of emissions as the electrical grid is fed by increasingly clean, renewable energies.

For a GSHP system, the incremental cost between a conventional system is the GHX. Since the GHX is already installed for the studied building, the incremental cost between a conventional system versus a GSHP is negligible. Additionally, EC glass often costs the same or less than conventional low-e glass after calculating the total cost of ownership and the additional costs attributed to controlling sun-light with interior shades, blinds and exterior sunshades (SageGlass, 2020a). Therefore, the NPV was solely calculated based on the annual energy cost savings. For a 30-year operating period based on the product life of the EC windows, the NPV was calculated at US$142,273.65 by using equations 3 and 4. This shows the advantage of integrating EC glass controls with the GHX to provide the highest return on investment for the stakeholders.

Chapter 4 – Ground heat exchanger thermal imbalance prevention using dynamic long-term ground temperature predictions

4.1 Methodology

In this study, we used a Trane Trace (Trane, 2019) building energy model to set the energy profile of the studied building for the initial year until a full annual dataset was achieved from monitoring. We created software on a remote server that collects measured data from the instrumentation installed on the studied building. We measured the live flowrates and temperatures which continuously updated the existing energy model profile and became progressively more accurate as measured energy loads account for variations in weather, changes in the building and operation of the system. We designed algorithms in the software to dynamically calculate the future predicted ground temperature and a control sequence to eliminate future system failure for the studied building. We calculated the system COP before and after mechanical improvements. The reduction in electricity consumption was calculated from the pumps operating efficiency, total capacity, and estimated run time. The reduction in electricity consumption was calculated for each hour of a given year and was included in the improved system COP calculation. To calculate the hourly COP's, the Carnot equations were used (Callendar, 1911):

$$COP = \frac{Q_H}{W_{in}} \tag{5}$$

where COP is the coefficient of performance, Q_H is the desired output in kW and W_{in} is the work required in kW. We determined the improved thermal balance from integrating with the roof-top make-

up air (MUA) unit through the building automation system (BAS). The additional heating load was determined by using Eq. 6 and the thermal balance was defined as the ratio between heating and cooling loads.

4.1.1 Project description

In this study, we installed the prototype energy meter on a 4786 m^2 office building located in Winnipeg, Manitoba, Canada. The office building was heated and cooled with a distributed water to air heat pump system utilizing a horizontally directionally drilled GHX located underneath the parking lot. To create an initial energy load set, a building energy model was developed. The building envelope U-factors used were: 1.42 W/m^2/K for the foundation, 0.14 W/m^2/K for the roof, 0.26 W/m^2/K for the wall and 1.82 W/m^2/K for the windows. The windows were modelled with a shading coefficient of 0.27. All envelope related inputs for the energy model were obtained from the final construction drawings. The ventilation and exhaust rates were taken from the ASHRAE 62.1 standard (ASHRAE, 2007). The hourly schedules were based on operating times between 8 am to 5 pm during weekdays, 8 am to 4 pm on Saturdays and closed on Sundays. The people, lighting, hourly schedules, and load densities were based on information gathered from the office building staff (Table 7).

Table 7: Room type with occupancy, lighting, and equipment internal load density information.

Room type	Internal Load Density		
	Occupancy	Lighting (W/m^2)	Equipment
ATM room	0 people	10.7	350 W
IT open office	4 people	10.7	750 W
Locker room	0.37 m^2/ person	10.7	0 W/m^2
Meeting room	10 people	10.7	250 W

Corridor/Vestibule	0 people	10.7	0 W/m^2
Data room	0 people	10.7	10.7 W/m^2
Receiving	2 people	10.7	200 W
Office space	2 people	10.7	175 W
Atrium	25 people	10.7	2.6 kW
Servery	4 people	13.5	750 W
Staff room	20 people	10.7	0 W/m^2
Mechanical room	0 people	10.7	0 W/m^2
Storage	0 people	10.7	0 W/m^2
Waiting area	2 people	10.7	0 W/m^2
Washroom	0 people	10.7	0 W/m^2

The GHX was horizontal directionally drilled with two rows of u-tubes installed in each trench (Fig. 9), the heat exchange fluid was a 20% propylene glycol and water blend whereas the other main parameters used can be seen in Table 8. The input parameters for the GHX were based on the as-built specifications and construction drawings.

Table 8: GHX design parameters.

Parameter	Value
Borehole number	72
Vertical borehole separation	2.4 m
Horizontal borehole separation	0.91 m
Borehole diameter	102 mm
Borehole depth	5.5 m
Borehole length	70 m

Design flow rate	3.2 l/hr/kW
Flow type	Turbulent
Ground thermal conductivity	1.09 W/m·K
Ground diffusivity	0.037 m^2/day
Thermal resistance	0.10 m·K/W
Undisturbed ground temperature	7.2°C

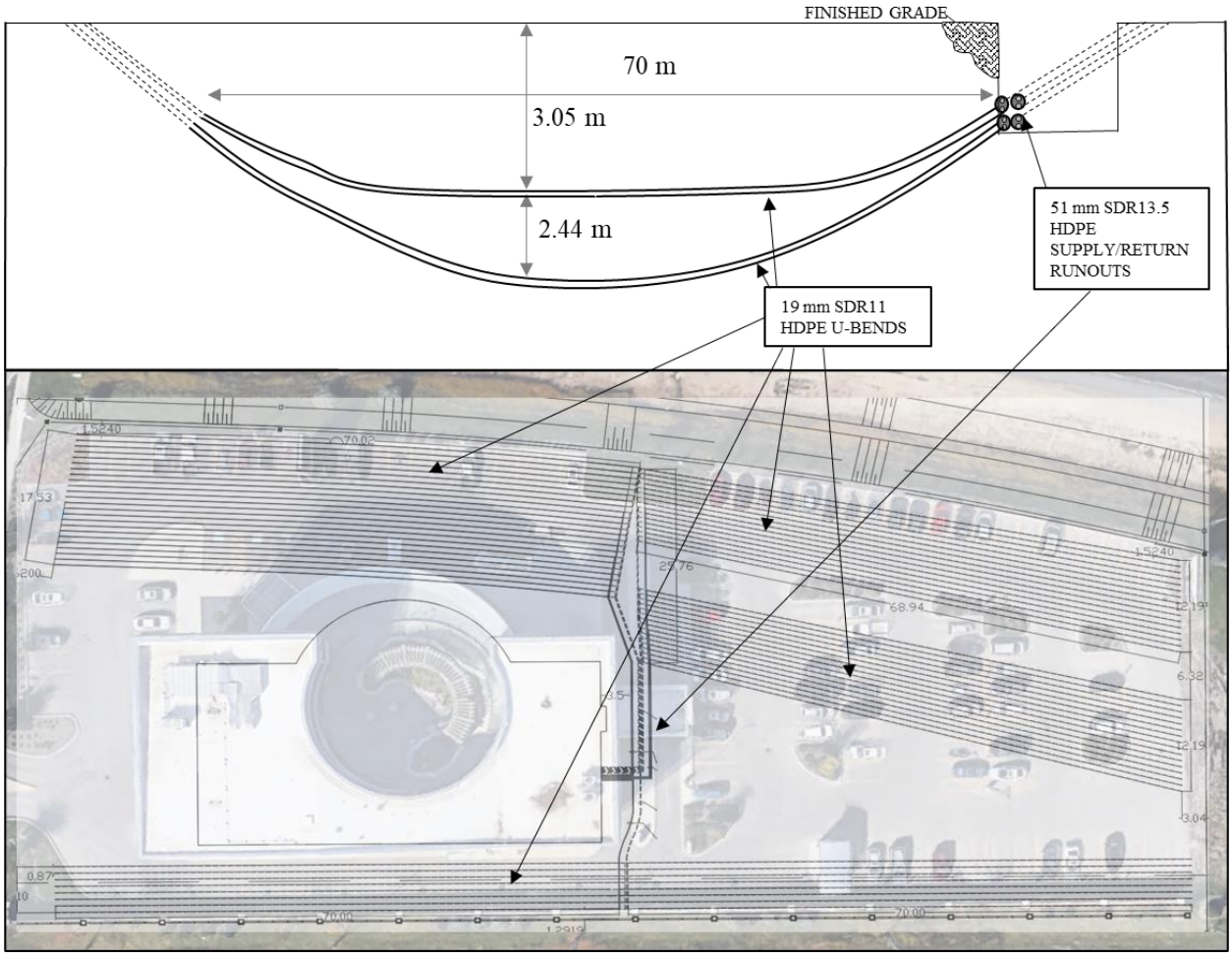

Figure 9: Section and plan view of horizontally drilled GHX.

4.1.2 Instrumentation description

The prototype components included a flow meter, temperature sensors, flow transducers, control box and antenna as seen in Fig. 10. The flow transducers were installed on the main manifold of the GHX and connected to the flow meter. The flow meter used a 4-20mA analog signal with an accuracy of 1%. The maximum flow rate was set to 45.5 m^3/hr. The flow meter and temperature sensors were wired to the control box which sent data to an external server through a Wi-Fi connection obtained from the antenna. The thermocouples were installed on the inlet and outlet of the GHX to obtain a temperature differential reading and had an accuracy of ± 0.5°C.

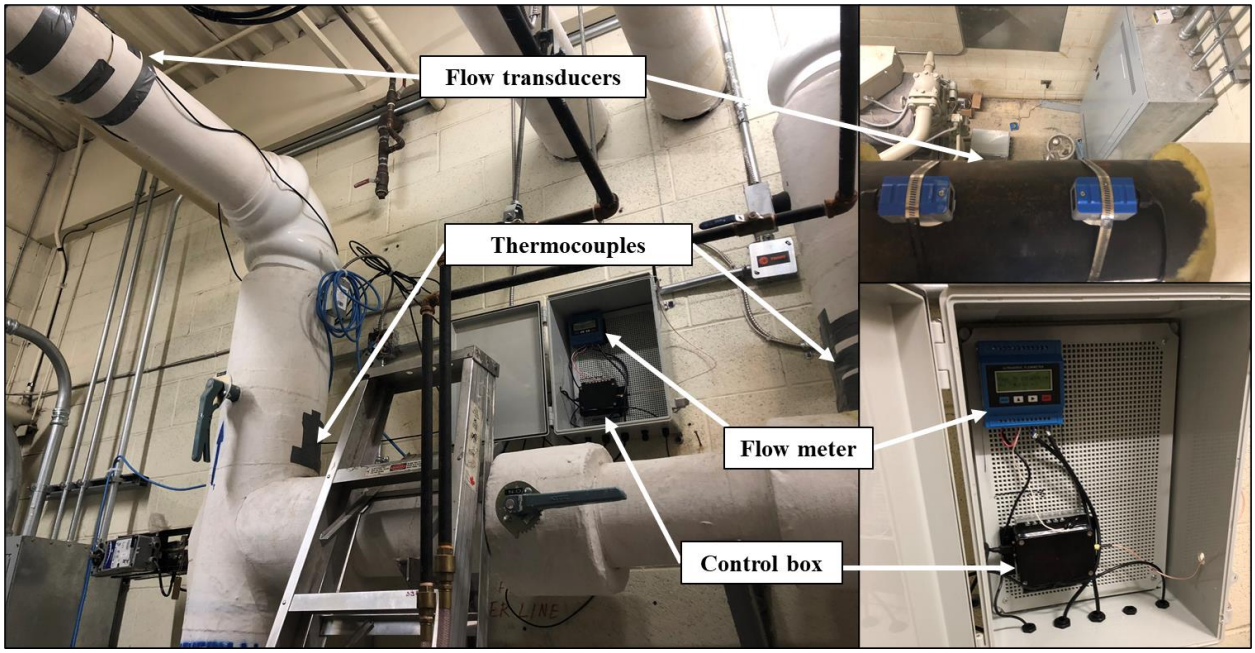

Figure 10: Pictures of installed prototype instrumentation.

4.1.3 Software description

The standalone prototype used a 2.4GHz Wi-Fi module that connected over TCP/IP and standard routers. The module was configured to function as a client that sends data to the server at predefined,

regularly spaced time intervals of 10 minutes. The prototype used a Linux VPS server account as the cloud-based platform for the data collection and calculations. The main site used a local NoSQL data-base that allows for horizontal scalability. The prototype was also designed for compatibility with a BAS by communicating via BACnet to control auxiliary heating and cooling devices based on the measured GHX temperatures (Fig. 11).

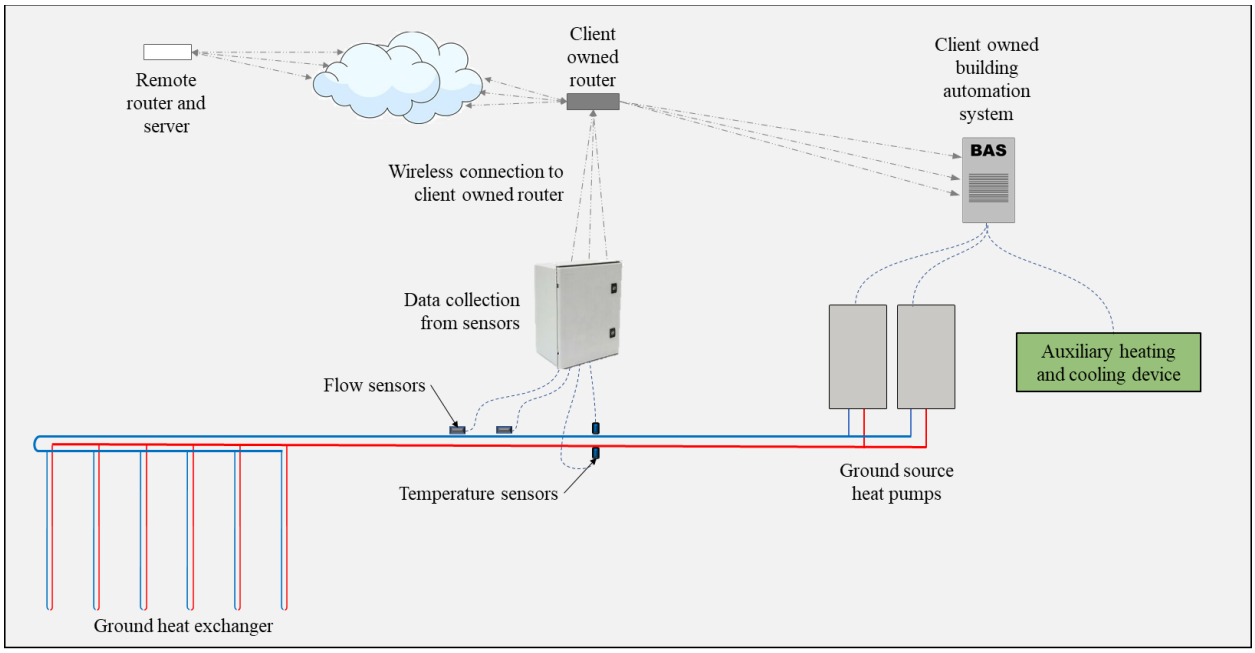

Figure 11: Conceptual design of energy meter with dynamic predictive capabilities.

4.1.3.1.Governing equations

To calculate the net energy loads extracted and injected into the GHX, the following equation was used (Bergman, Lavine, Incropera, & Dewitt, 2007):

$$q = \dot{Q} C_p \rho \Delta T \tag{6}$$

where q is the amount of heat transfer in W, $\dot{Q}$ is the volumetric flow rate in m^3/s, C_p is the specific heat of the heat exchange fluid in kJ/kg·°C, ρ is the density of the fluid in kg/m^3 and ΔT is the temperature difference in the GHX between the inlet and outlet. To dynamically predict the future temperature of the GHX based on the monitored energy loads, the following equation was used (Gonet, 2010):

$$R_b = \frac{1}{\dot{W}}(T_f - T_0) - \frac{1}{(4\pi\lambda)}\left[\ln(t) + \ln\left(\frac{4\alpha}{{r_0}^2}\right) - \gamma\right] \text{ where } T_f = \frac{T_{in}+T_{out}}{2} \quad \& \quad \dot{W} = \frac{q}{H} \tag{7}$$

where R_b is the thermal resistance between the heat exchange fluid and the borehole wall in m·K/W, T_o is the mean temperature of profile in K, T_f is the mean of the inlet and outlet fluid temperatures of the heat exchanger in K, $\dot{W}$ is the heat transfer rate in W/m, H is the active length of the borehole in m, λ is the thermal conductivity in W/m·K, t is time in days, r_o is the borehole radius in m, α is the thermal diffusivity in m^2/day and γ is Euler's constant taken as 0.5772.

4.2 Results and discussions

4.2.1 Monitored data analysis

Flow rate, inlet temperature and outlet temperature data were collected from January 30th to July 30th, 2021, in 10-minute intervals. Fig. 12 shows a minimum and maximum GHX inlet temperature of 3.1°C and 34.4°C, respectively. Throughout the same monitoring period, the minimum and maximum outdoor air temperature is -37.9°C and 36.1°C, respectively. The 31.3°C change in GHX inlet temperature compared to the 74°C change in outdoor air temperature can be attributed to the storage capabilities of the soil surrounding the GHX. The stratigraphy at depths up to 20 m consists of glaciolacustrine clay in the Winnipeg region which has poor thermal property characteristics due to low density and small pore spaces (Betcher, Grove, & Pupp, 1995). Moreover, the minimum inlet and outlet temperatures of

the GHX should range from -1.1°C to 1.7°C throughout peak heating months from the GSHP system operation whereas the maximum inlet and outlet temperatures throughout the cooling months should range from -26.7°C to 32.2°C (Kavanaugh & Rafferty, 2014). The relatively high inlet and outlet GHX temperatures can be attributed to the cooling dominate building that was studied. Since the building rejects more heat to the GHX than extracts annually, the inlet and outlet temperatures are higher than originally designed for.

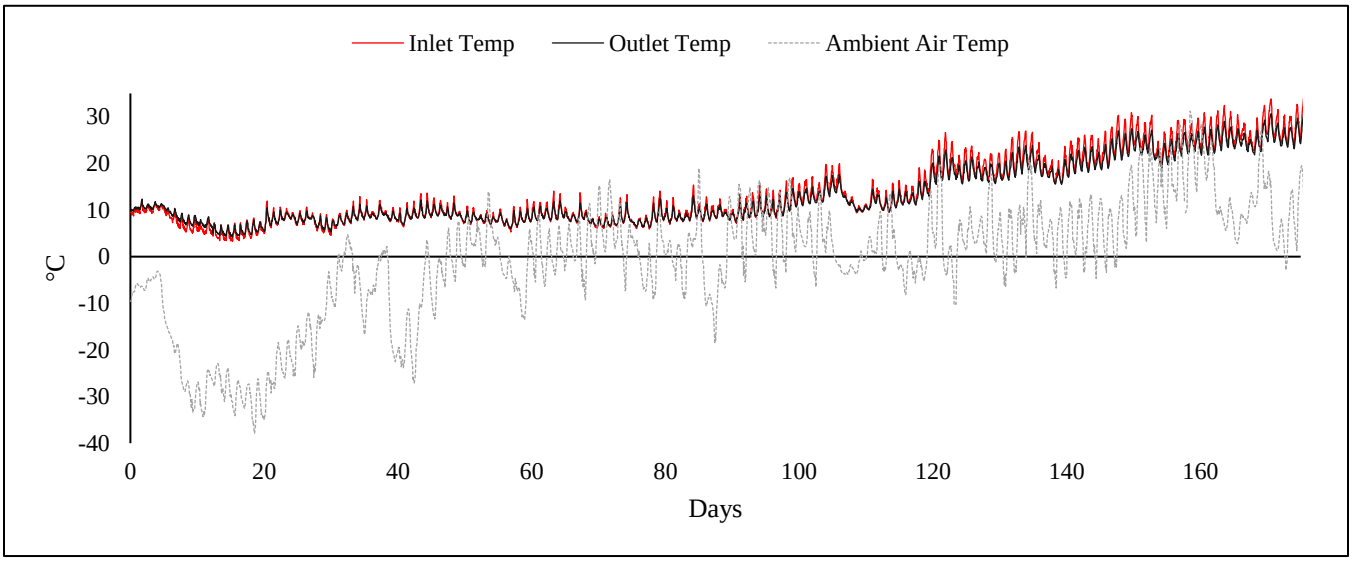

Figure 12: Monitored inlet and outlet temperatures of the GHX and the average outdoor air temperature.

The temperature difference between the inlet and outlet of the GHX was plotted against the flow rate through the GHX and can be seen in Fig. 13. Throughout the heating season, an optimal temperature difference is 2.2°C whereas the average temperature difference throughout the monitored period during the heating season was 0.14°C. Throughout the cooling season, an optimal temperature difference is 3.6°C whereas the average temperature difference throughout the monitored period during the cooling season was 1.5°C. This implies the flow rate through the GHX was too high. The average flow rate throughout

the monitored period was 34.8 m^3/hr. The mechanical design of the GSHP system has a constant speed circulation pump that circulates heat exchange fluid through an independent GHX loop attached to the building loop with a modulating valve. When the building loop is above or below the temperature set-points, the modulating valve opens and allows heat transfer between the building loop and the GHX loop. Currently, when the building loop does not require additional heat transfer, the circulation pump on the GHX continues to circulate heat exchange fluid which injects pump energy into the GHX. Based on the 3.7 kW circulation pump at 80% efficiency, the energy injected into the ground annually through the heat exchange fluid is 25,930 kWh. This increases the thermal imbalance between heating and cooling loads which creates a less efficient and unsustainable GSHP system. Since the GHX is horizontal directionally drilled, it can take advantage of shallower depths and ambient energy dissipation. Nonetheless, heat storage capacity is prevalent due to the installed GHX depth of 3.1 and 5.5 m. Installing a variable frequency drive on the existing GHX circulation pump would decrease the amount of energy injected to the GHX and decrease annual operating costs due to decreased pumping energy. Fig. 14 shows the measured energy flow into and out of the GHX. The total amount of energy extracted from the ground was 104,197 kWh whereas the total amount of energy injected into the ground was 835,238 kWh which indicates a cooling dominate building throughout the monitored period. The insight provided from the GSHP monitoring system allows for the potential of operating savings and reduction of ground temperature drift. This shows the importance of developing a dynamic GSHP monitoring system that can alert building operators of unsustainable temperature trends.

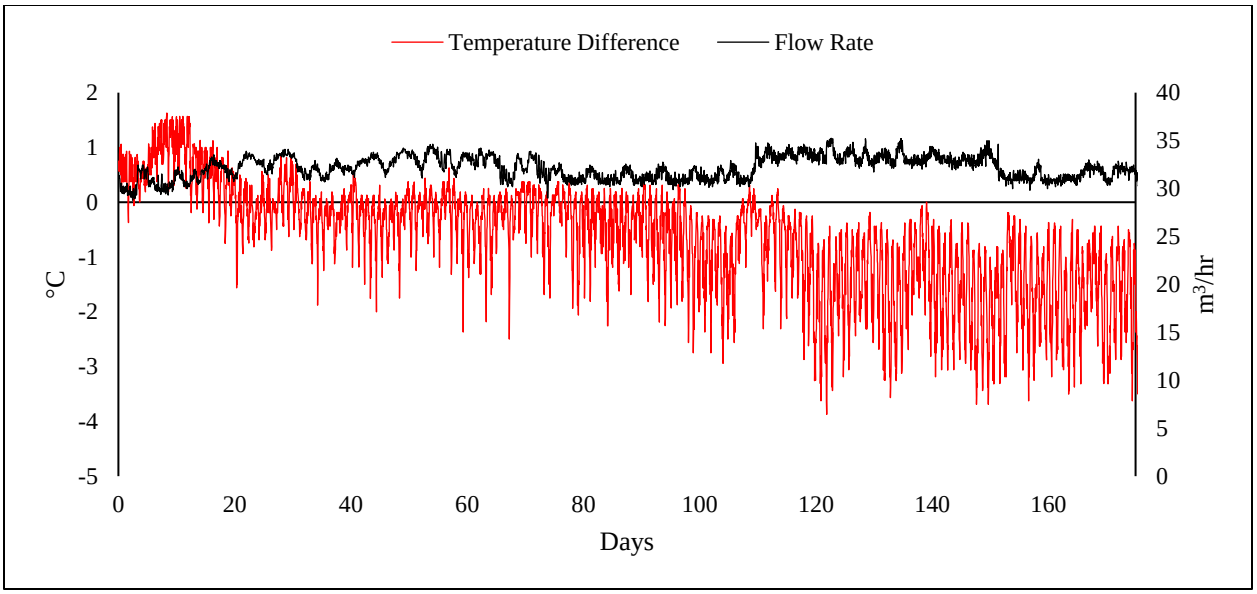

Figure 13: Monitored temperature difference from the inlet and outlet of the GHX and flow rate through the GHX.

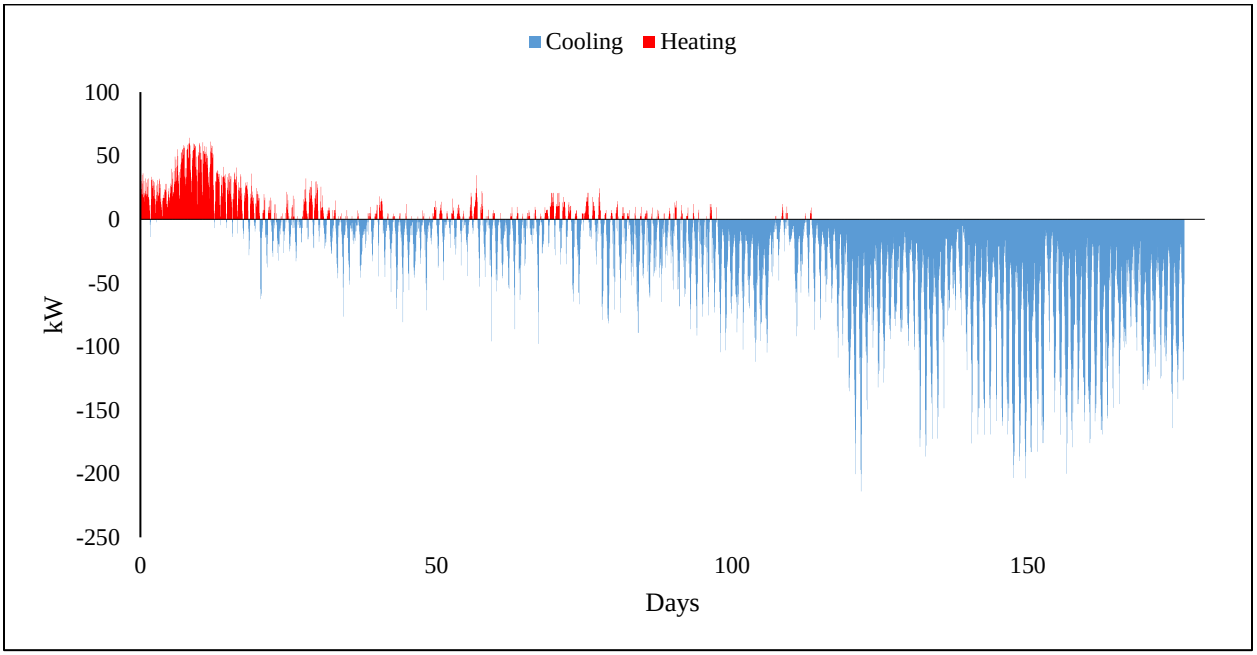

Figure 14: Measured net energy flow into and out of the GHX.

4.2.2 Energy load comparison

Fig. 15 shows a correlation coefficient of 0.37 between the initial modelled and current monitored energy loads. The root square mean error between the modelled and measured heating and cooling loads in the winter months was 16.7 kW and 44.3 kW, respectively. The root square mean error between the modelled and measured heating and cooling loads in the summer months was 23.3 kW and 69.2 kW, respectively. The authors attribute the increased difference in cooling load between measured and modelled compared to the heating load to climate change. The average measured dry bulb temperature for the studied location in winter and summer months were -7.2°C and 15.9°C, respectively. Energy models are often created using typical meteorological year (TMY3) files. The average dry bulb temperature from the TMY3 file for the location of the monitored building in winter and summer months were -10.8°C and 14.8°C, respectively. This shows the affect of climate change and its impact on dry bulb temperature which influences heating and cooling loads. Additional factors that could affect the difference in modelled and measured load sets are the hours of operation, occupancy, and other variables which influence the internal heat gains.

The purpose of Fig. 15 was to show the difference in initial energy models used for new construction projects compared to the actual monitored data once the building is operational since energy models are always created years prior to the beginning of the monitoring period of the GHX. Building mechanical systems are typically sized based on detailed energy models and detailed energy models are primarily built based on assumptions on how the building will operate once built. Moreover, the building manager can change the hours of operation, occupancy, and other variables which affect the internal load densities. For a conventional boiler/cooling tower system the annual energy loads are trivial as the system can be oversized using peak loads with minimal repercussions whereas a GSHP system acts like a utility where the energy source and supply is designed. If an annual thermal imbalance develops, it must

be corrected to sustain high efficiency throughout the systems operating lifetime. The ability to monitor and predict future ground temperature trends based on real time energy loads is critical for the assured sustainability of a GSHP system.

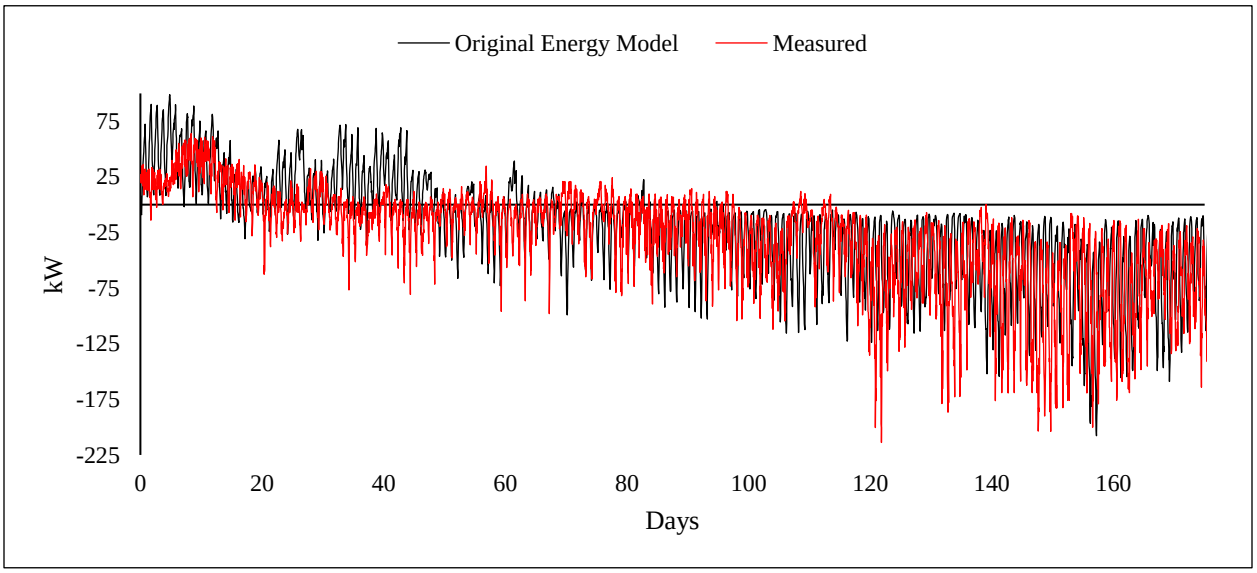

Figure 15: Comparison of monitored energy loads and simulated energy loads.

4.2.3 Long-term GHX temperature calculations

Fig. 16 shows the calculated GHX temperatures over the next 20 years. An increasing GHX temperature trend is shown which is attributed to more heat being rejected than extracted from the ground. The maximum GHX temperature was 19°C in the first year and increased to 36°C by year 16. This trend is unsustainable if the current mechanical system operation continues and will cause the system to become inefficient by year 16 from high inlet temperatures to the heat pumps. The red dotted line at 35°C in Fig. 16 represents the upper limit of efficient operation. Predicting the future temperature trend based on real-time energy loads allows for pre-emptive operational or mechanical changes to be made to the system. This approach can be extrapolated to any GSHP system to eliminate system failure, increase confidence and reliability, which will ultimately grow the GSHP industry.

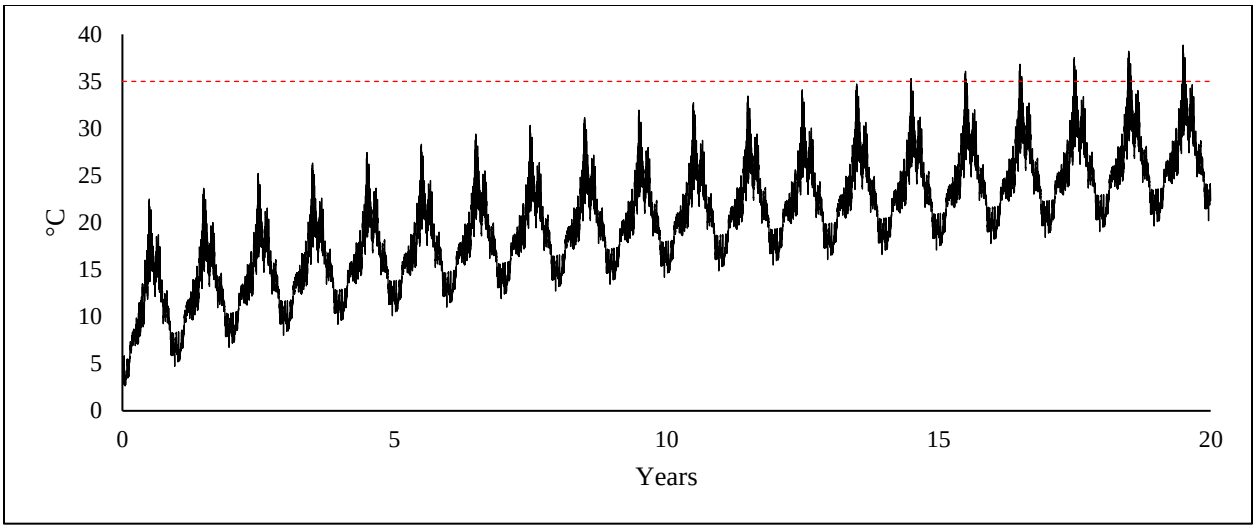

Figure 16: 20-year GHX temperature trend calculation.

4.2.4 System efficiency

The constant speed circulation pump on the studied building increased energy injected to the GHX and electricity consumption. By adding a variable frequency drive to the circulation pump, this reduced the system energy consumption by 24%, which increased the heating and cooling COP as seen in Table 9. The amount of power consumed by the heat pumps depends on the temperature difference between the source and load side. The heating COP is higher than the cooling COP due to the higher source side temperatures from the GHX. Since the building is cooling dominate, more heat is rejected to the GHX than extracted. As shown in Fig. 16, this increases the ground temperature over time which allows the heat pumps to consume less power when heating, and more power when cooling. The system COP increased when a variable frequency drive was added to the circulation pump since it used less energy to deliver the same amount of heating and cooling.

Table 9: Heating and cooling COP comparison between existing and improved building mechanical systems.

	Improved	Existing
Cooling (COPc)	3.4	2.8
Heating (COP)	6.9	5.3

4.2.5 Integration to building automation system

BAS's control various components of a buildings mechanical system. In the studied building, the BAS controls the roof-top natural gas MUA unit. The MUA unit heats up the outdoor air to reduce the heating load on the GSHP system. By integrating the prototype with the BAS, the amount of heating performed by the GSHP system can be adjusted based on the MUA unit set-point temperature. Since the studied building is cooling dominate, allowing the GSHP system to perform more heating would increase the balance between the heating and cooling loads. Fig. 17 represents the control sequence developed for the studied building. By lowering the set-point temperature of the MUA unit from 12.8°C to 4.8°C, the amount of heating performed by the GSHP system increased by 49,230 kWh which maintained the future 20-year GHX temperature below 32°C. As climate change continues to affect building heating and cooling loads, the prototype will collect data and dynamically calculate the future GHX temperatures which will signal the MUA unit if the calculated future GHX temperatures fall out of set-point. This concept can be applied to any GSHP system with an auxiliary heating or cooling device to eliminate a GHX thermal imbalance and assure a sustainable system throughout climate change which will shift the perception that GSHP systems are unreliable.

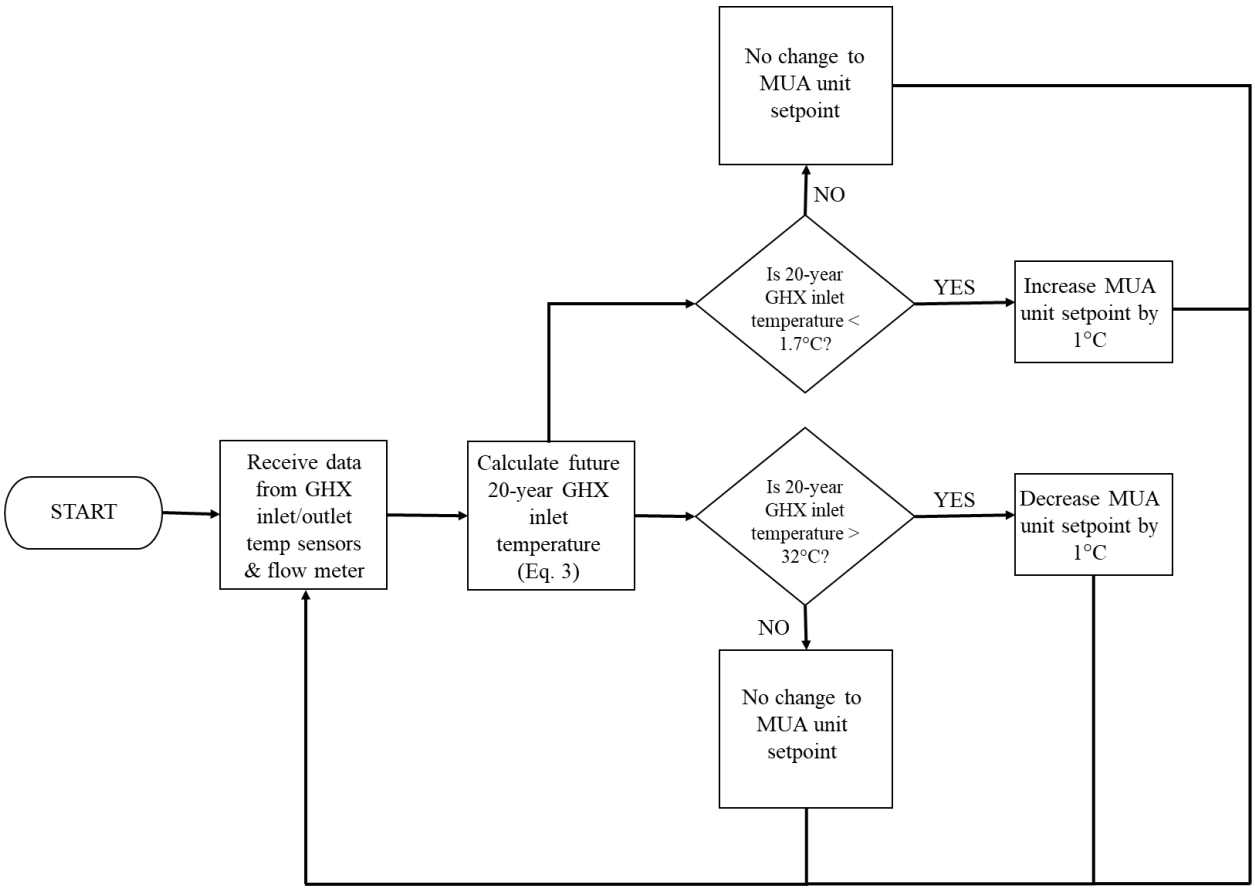

Figure 17: Sequential function chart for control sequence for mitigating GHX failure.

Chapter 5 – Conclusion and Recommendation for Future Work

5.1 Conclusion

The first objective in this thesis focused on determining the feasibility of integrated GSHP system with EC window glazing to optimize long-term system performance and prevent thermal imbalance of the ground heat exchanger. To determine the feasibility of implementing the system, a detailed building energy model was developed and simulated with various SHGC's to model EC glass windows. Additionally, four weather files were used to create the energy load sets: the base weather file, projected 2050 weather for RCP 2.6, RCP 4.5, and RCP 8.5 climate change scenarios. A GHX model was also developed to analyze the long-term temperature trends of the various energy load sets and to calculate the system efficiencies. This study found that:

- The integrated GSHP system with EC windows was proven feasible and a conceptual control sequence and design was developed.
- The annual cooling demand decreased by 32% between the clear glass state versus the fully tinted state and remained within an acceptable 20-year range for the maximum EWT to the heat pumps for the fully tinted state.
- It was recommended to increase the GHX capacity to 200 boreholes at 45.7 m in 2040 when the life cycle of the heat pumps are complete which limits the max EWT to below 35°C for a worst-case scenario of RCP 8.5 from 2040-2060.
- The average COP's for heating, cooling and simultaneous loads were 5.3, 8.5, and 7.5 for the clear glass state and 6.4, 9.2 and 7.3 for the fully tinted state, respectively.

- The integrated GSHP system reduced CO_2 emissions by 30% and the 30-year NPV was US$142,273.65.

More importantly, this study provided a conceptual design methodology for ensuring future sustainable GSHP systems. Since the GHX acts as a battery, it is effective to design a mechanical system with a supplementary device that assists in balancing the heating and cooling loads for the building which can indirectly recharge the GHX when needed. Integrated controls between the supplementary device and the GSHP system creates a cost effective and sustainable design that can be monitored and managed for long-term optimization.

The second objective of the thesis was to develop a software and hardware package that dynamically calculates future ground heat exchanger temperatures to avoid thermal imbalance and future system failure. It can be concluded from the research that monitoring the energy flow of a GHX is critical and dynamic future GHX temperature calculations allow for pre-emptive mechanical and operational changes to eliminate system failure from temperature drift. It was determined that the building was cooling dominate and if the current mechanical system operation continues it will cause the system to become inefficient by year 16 from high inlet temperatures to the heat pumps. A control sequence was developed for mitigating ground heat exchanger failure on the studied building. It was also determined by adjusting the set-point temperature of the make-up air unit from 12.8°C to 4.8°C, the amount of heating performed by the ground source heat pump system increased by 49,230 kWh which sustained the future 20-year ground heat exchanger temperature below 32°C. Lastly, by adding a variable frequency drive to the circulation pump, it was shown that the system energy consumption reduced by 24%, which increased the system heating and cooling COP to 6.9 and 3.4, respectively.

The main outcome from this research was a hardware and software package that can be used on any GSHP system to assure sustainability over time and eliminate system failure. The GSHP industry has

frequently received a poor reputation due to system failure which has limited growth. Eliminating GSHP system failure will assist in growing the industry which will lead to the electrification of buildings and ultimately reduce global greenhouse gas emissions and support the fight of climate change.

5.2 Recommendations for future work

The limitations of this study were the absence of convective heat transfer for determining the 20-year maximum EWT based on the GHX size. This leads to conservative results which were acceptable for the first objective of the thesis. The annual steady state of the tint levels in the first objective was deemed a limitation since, the change in tint levels will be transient. The six-month dataset was deemed a limitation for the second objective since half of the annual dataset was theoretical. Future studies will incorporate monitored annual ground heat exchanger energy loads sets showing optimization through auxiliary heating and cooling devices controlled based on future calculated ground heat exchanger temperatures.

Bibliography

Alaica, A. A., & Dworkin, S. B. (2017). Characterizing the effect of an off-peak ground pre-cool control strategy on hybrid ground source heat pump systems. *Energy and Buildings*, *137*, 46–59. http://doi.org/10.1016/j.enbuild.2016.12.003

ASHRAE. (2007). *Ventilation for acceptable indoor air quality*. *ASHRAE Standard* (Vol. 2007).

ASHRAE. (2016). *ASHRAE 90.1 - Energy Standard for Buildings Except Low-Rise Residential Buildings*.

ASHRAE. (2017). *ASHRAE 55 - Thermal Environmental Conditions for Human Occupancy*.

Beckers, K. F., Aguirre, G. A., & Tester, J. W. (2018). Hybrid ground-source heat pump systems for cooling-dominated applications: Experimental and numerical case-study of cooling for cellular tower shelters. *Energy and Buildings*, *177*, 341–350. http://doi.org/10.1016/j.enbuild.2018.08.005

Bergman, T. L., Lavine, A. S., Incropera, F. P., & Dewitt, D. P. (2007). *Fundamental of Heat and Mass Transfer* (7th ed.). Hoboken: John Wiley & Sons, Inc.

Betcher, R., Grove, G., & Pupp, C. (1995). *Groundwater in Manitoba: Hydrogeology, Quality Concerns, Management*.

Bush, E. and Lemmen, D. S. (2019). *Canada's Changing Climate*. Ottawa.

Callendar, H. L. (1911). The Caloric Theory of Heat and Carnots Principle. *Proceedings of the Physical Society of London*.

Craik, N. (2017). Developing a National Strategy for Climate Engineering Research in Canada. *Climate Engineering*, (153), 24.

Cuomo, G. A. M. (2021). Governor Cuomo Announces Nearly $ 4 Million Awarded to Grow Community Heat Pump Networks Across New York State. *Governor's Press Office*. Albany, NY. Retrieved from https://www.governor.ny.gov/news/governor-cuomo-announces-nearly-4-million-awarded-grow-community-heat-pump-networks-across-new

Dai, L., Li, S., DuanMu, L., Li, X., Shang, Y., & Dong, M. (2015). Experimental performance analysis of a solar assisted ground source heat pump system under different heating operation modes. *Applied Thermal Engineering*, *75*, 325–333. http://doi.org/10.1016/j.applthermaleng.2014.09.061

DeForest, N., Shehabi, A., O'Donnell, J., Garcia, G., Greenblatt, J., Lee, E. S., … Milliron, D. J. (2015). United States energy and CO2 savings potential from deployment of near-infrared electrochromic window glazings. *Building and Environment*, *89*, 107–117. http://doi.org/10.1016/j.buildenv.2015.02.021

Energy Star. (2020). *Energy Star Guidelines*.

Eskilson, P. (1987). *Thermal Analyses of Heat Extraction Boreholes*. Lund Institute of Technology.

Fernandes, L. L., Lee, E. S., & Ward, G. (2013). Lighting energy savings potential of split-pane electrochromic windows controlled for daylighting with visual comfort. *Energy and Buildings*, *61*, 8–20. http://doi.org/10.1016/j.enbuild.2012.10.057

FRED. (2020). Federal Reserve Bank of St. Louis.

Gaia Geothermal. (2020). Ground Loop Design V10.

Gonet, A. (2010). Modification of Method of Interpreting Thermal Response Test of Borehole Heat Exchanger. *B-Dig.Iie.Org.Mx*, (April), 25–29. Retrieved from http://b-dig.iie.org.mx/BibDig/P10-0464/pdf/2828.pdf

Hamstra, S. A. (2019). SYSTEM FOR OPTIMIZATION OF BUILDING HEATING AND COOLING SYSTEMS. United States of America.

Hwang, J., Song, D., & Lee, T. (2020). The Effect of Coupling Solar Thermal System and Geothermal Heat Pump Systems in Areas with Unbalanced Heating and Cooling Demand. *Energies*.

Hwang, Y., Lee, J. K., Jeong, Y. M., Koo, K. M., Lee, D. H., Kim, I. K., … Kim, S. H. (2009). Cooling performance of a vertical ground-coupled heat pump system installed in a school building. *Renewable Energy*, *34*(3), 578–582. http://doi.org/10.1016/j.renene.2008.05.042

Javad, K., & Navid, G. (2019). Thermal comfort investigation of stratified indoor environment in displacement ventilation: Climate-adaptive building with smart windows. *Sustainable Cities and Society*, *46*, 101354. http://doi.org/https://doi.org/10.1016/j.scs.2018.11.029

Kavanaugh, S., & Rafferty, K. (2014). *Geothermal Heating and Cooling: Design of Ground-Source Heat Pump Systems* (2nd ed.). Atlanta.

Khosravi, A., & Syri, S. (2020). Modeling of geothermal power system equipped with absorption refrigeration and solar energy using multilayer perceptron neural network optimized with imperialist competitive algorithm. *Journal of Cleaner Production*, *276*, 124216. http://doi.org/10.1016/j.jclepro.2020.124216

Koohi-Fayegh, S., & Rosen, M. A. (2015). Three-Dimensional Analysis of the Thermal Interaction of Multiple Vertical Ground Heat Exchangers. *International Journal of Green Energy*, *12*(11), 1144–1150. http://doi.org/10.1080/15435075.2014.892876

Koohi-Fayegh, S., & Rosen, M. A. (2021). Modeling of vertical ground heat exchangers. *International Journal of Green*

Energy, *18*(7), 755–774. http://doi.org/10.1080/15435075.2021.1880913

Lee, E. S., Yazdanian, M., & Selkowitz, S. E. (2004). *The Energy-Savings Potential of Electrochromic Windows in the US Commercial Buildings Sector*. *Lawrence Berkeley National Laboratory*,.

Li, H., Nagano, K., Lai, Y., Shibata, K., & Fujii, H. (2013). Evaluating the performance of a large borehole ground source heat pump for greenhouses in northern Japan. *Energy*, *63*, 387–399. http://doi.org/10.1016/j.energy.2013.09.009

Lund, J. W., & Boyd, T. L. (2020). Direct utilization of geothermal energy 2020 worldwide review. *Geothermics*, *60*, 66–93. http://doi.org/10.1016/j.geothermics.2015.11.004

Luo, J., Rohn, J., Bayer, M., Priess, A., Wilkmann, L., & Xiang, W. (2015). Heating and cooling performance analysis of a ground source heat pump system in Southern Germany. *Geothermics*, *53*, 57–66. http://doi.org/10.1016/j.geothermics.2014.04.004

Meyerson, N. L. (1967). Heat quantity meter. United States Patent and Trademark Office.

Michopoulos, A., Zachariadis, T., & Kyriakis, N. (2013). Operation characteristics and experience of a ground source heat pump system with a vertical ground heat exchanger. *Energy*, *51*, 349–357. http://doi.org/10.1016/j.energy.2012.11.042

Montagud, C., Corberán, J. M., Montero, Á., & Urchueguía, J. F. (2011). Analysis of the energy performance of a ground source heat pump system after five years of operation. *Energy and Buildings*, *43*(12), 3618–3626. http://doi.org/10.1016/j.enbuild.2011.09.036

Oh, M., Tae, S., & Hwang, S. (2018). Analysis of heating and cooling loads of electrochromic glazing in high-rise residential buildings in South Korea. *Sustainability (Switzerland)*, *10*(4). http://doi.org/10.3390/su10041121

OTPCO. (2020a). *Electricity Carbon Intensity*.

OTPCO. (2020b). *Minnesota Commercial Rate Summary*.

Perham Natural Gas. (2020). *Perham Natural Gas*.

Qian, H., & Wang, Y. (2014). Modeling the interactions between the performance of ground source heat pumps and soil temperature variations. *Energy for Sustainable Development*, *23*, 115–121. http://doi.org/10.1016/j.esd.2014.08.004

Safa, A. A., Fung, A. S., & Kumar, R. (2015). Heating and cooling performance characterisation of ground source heat pump system by testing and TRNSYS simulation. *Renewable Energy*, *83*, 565–575. http://doi.org/10.1016/j.renene.2015.05.008

SageGlass. (2020a). Cost Savings. Retrieved November 3, 2011, from https://www.sageglass.com/en/benefits/cost-savings

SageGlass. (2020b). Learn More About SageGlass. Retrieved November 3, 2020, from https://www.sageglass.com/en/faqs

SageGlass. (2020c). *Performance Data*.

Sagia, Z., Rakopoulos, C., & Kakaras, E. (2012). Cooling dominated Hybrid Ground Source Heat Pump System application. *Applied Energy*, *94*, 41–47. http://doi.org/10.1016/j.apenergy.2012.01.031

Sarbu, I., & Sebarchievici, C. (2014). General review of ground-source heat pump systems for heating and cooling of buildings. *Energy & Buildings*, *70*, 441–454. http://doi.org/10.1016/j.enbuild.2013.11.068

Shang, Y., Dong, M., & Li, S. (2014). Intermittent experimental study of a vertical ground source heat pump system. *Applied Energy*, *136*, 628–635. http://doi.org/10.1016/j.apenergy.2014.09.072

Stull, R. (2011). Wet-bulb temperature from relative humidity and air temperature. *Journal of Applied Meteorology and Climatology*, *50*(11), 2267–2269. http://doi.org/10.1175/JAMC-D-11-0143.1

Tavares, P., Bernardo, H., Gaspar, A., & Martins, A. (2016). Control criteria of electrochromic glasses for energy savings in mediterranean buildings refurbishment. *Solar Energy*, *134*, 236–250. http://doi.org/10.1016/j.solener.2016.04.022

Trane. (2019). TRACE 700 6.3.4.

U.S. Department of Energy. (2011). Guide to Geothermal Heat Pumps. *Energy Efficiency and Renewable Energy*, *DOE/EE-038*, 2.

U.S. Energy Information Administration. (2012). *2012 Commercial Buildings Energy Consumption Survey*.

U.S. Energy Information Administration. (2019). *U.S. primary energy consumption by source and sector*. Retrieved from https://www.eia.gov/totalenergy/data/monthly/pdf/flow/css_2017_energy.pdfpdf

United Nations. (2019). *United Nations Climate Change Annual Report 2019*.

United States Environmental Protection Agency. (2017). Greenhouse Gases Equivalencies Calculator - Calculations and References. Retrieved from https://www.epa.gov/energy/greenhouse-gases-equivalencies-calculator-calculations-and-references

US Inflation Calculator. (2020). US Inflation Calculator. Retrieved from https://www.usinflationcalculator.com/inflation/historical-inflation-rates/

Wan, K. K. W., Li, D. H. W., Pan, W., & Lam, J. C. (2012). Impact of climate change on building energy use in different climate zones and mitigation and adaptation implications. *Applied Energy*, *97*, 274–282. http://doi.org/10.1016/j.apenergy.2011.11.048

Wang, X., Cui, P., Zhang, W., Zhou, X., & Li, L. (2017). Optimal Design methods and experimental validation for hybrid ground source heat pump system with gas boiler. *Procedia Engineering*, *205*, 4149–4156. http://doi.org/10.1016/j.proeng.2017.10.159

Yan, L., Hu, P., Li, C., Yao, Y., Xing, L., Lei, F., & Zhu, N. (2016). The performance prediction of ground source heat pump system based on monitoring data and data mining technology. *Energy and Buildings*, *127*, 1085–1095. http://doi.org/10.1016/j.enbuild.2016.06.055

Yang, W., Liang, X., Shi, M., & Chen, Z. (2014). A Numerical Model for the Simulation of a Vertical U-Bend Ground Heat Exchanger Used in a Ground-Coupled Heat Pump. *International Journal of Green Energy*, *11*(7), 761–785. http://doi.org/10.1080/15435075.2013.829474

You, T., Wang, B., Wu, W., Shi, W., & Li, X. (2015). Performance analysis of hybrid ground-coupled heat pump system with multi-functions. *Energy Conversion and Management*, *92*, 47–59. http://doi.org/10.1016/j.enconman.2014.12.036

You, T., Wu, W., Shi, W., Wang, B., & Li, X. (2016). An overview of the problems and solutions of soil thermal imbalance of ground-coupled heat pumps in cold regions. *Applied Energy*, *177*, 515–536. http://doi.org/10.1016/j.apenergy.2016.05.115

Zhao, D., Deng, S., Zhao, L., Xu, W., Wang, W., Nie, X., & Chen, M. (2020). Overview on artificial intelligence in design of Organic Rankine Cycle. *Energy and AI*, *1*, 100011. http://doi.org/10.1016/j.egyai.2020.100011

Zhou, W., Pei, P., Mao, R., Qian, H., Hu, Y., & Zhang, J. (2020). Selection and techno-economic analysis of hybrid ground source heat pumps used in karst regions. *Science Progress*, *103*(2), 1–17. http://doi.org/10.1177/0036850420921682